ARTICLE

https://doi.org/10.1038/s41586-018-0649-2

Targeted neurotechnology restores walking in humans with spinal cord injury

Fabien B. Wagner[1,2,15], Jean-Baptiste Mignardot[1,2,15], Camille G. Le Goff-Mignardot[1,2,15], Robin Demesmaeker[1,2], Salif Komi[1,2], Marco Capogrosso[3], Andreas Rowald[1,2], Ismael Seáñez[1,2], Miroslav Caban[4,5], Elvira Pirondini[1,2,6], Molywan Vat[7], Laura A. McCracken[1,2], Roman Heimgartner[1,2], Isabelle Fodor[2], Anne Watrin[4], Perrine Seguin[1,2], Edoardo Paoles[4], Katrien Van Den Keybus[2], Grégoire Eberle[2], Brigitte Schurch[2], Etienne Pralong[7], Fabio Becce[8], John Prior[9], Nicholas Buse[10], Rik Buschman[10], Esra Neufeld[11], Niels Kuster[11,12], Stefano Carda[2], Joachim von Zitzewitz[4], Vincent Delattre[4], Tim Denison[10,13], Hendrik Lambert[4], Karen Minassian[1,2,16], Jocelyne Bloch[2,7,14,16] & Grégoire Courtine[1,2,7,14,16]*

Spinal cord injury leads to severe locomotor deficits or even complete leg paralysis. Here we introduce targeted spinal cord stimulation neurotechnologies that enabled voluntary control of walking in individuals who had sustained a spinal cord injury more than four years ago and presented with permanent motor deficits or complete paralysis despite extensive rehabilitation. Using an implanted pulse generator with real-time triggering capabilities, we delivered trains of spatially selective stimulation to the lumbosacral spinal cord with timing that coincided with the intended movement. Within one week, this spatiotemporal stimulation had re-established adaptive control of paralysed muscles during overground walking. Locomotor performance improved during rehabilitation. After a few months, participants regained voluntary control over previously paralysed muscles without stimulation and could walk or cycle in ecological settings during spatiotemporal stimulation. These results establish a technological framework for improving neurological recovery and supporting the activities of daily living after spinal cord injury.

Spinal cord injury (SCI) disrupts communication within the nervous system, leading to the loss of essential neurological functions. At present, activity-based therapies are the only medical practices that can be used to enhance recovery[1–3]. The volitional production of active movements during training promotes reorganization of neuronal pathways and thereby augments recovery[4,5]. However, the most affected patients, who fail to produce active movements voluntarily, experience minimal benefits from these therapies[1].

This situation has prompted the development of multifaceted neurotechnologies[6], such as lower limb exoskeletons, bodyweight support systems, functional electrical stimulation of muscles, and spinal cord neuromodulation therapies, all of which share the same goal: to enable patients to sustain active movements during training to enhance the reorganization of neuronal pathways[4]. Three decades of clinical research using these neurotechnologies suggested that epidural electrical stimulation (EES) of the spinal cord may be pivotal to achieve this goal[7–10]. EES not only enables the brain to exploit spared but functionally silent descending pathways in order to produce movements of paralysed limbs[11,12], but also improves the ability of the spinal cord to translate task-specific sensory information into the muscle activity that underlies standing and walking[9,10,12–16].

To harness the therapeutic potential of EES, we studied its underlying mechanisms. We found that EES activates motor neurons by recruiting proprioceptive circuits within the posterior roots of the spinal cord[17–20]. This understanding translated into EES protocols that target individual posterior roots to access the motor neuron pools located in the spinal cord segment innervated by each root[21]. To engage motor neurons at the appropriate time, spatially selective EES trains are delivered with timing that coincides with the intended movement. Compared to empirical stimulation protocols, spatiotemporal EES enhances the potency of leg movements, which enabled weight-bearing locomotion in animal models of leg paralysis[21–23]. When combined with overground locomotor training enabled by a gravity-assist device[24], this stimulation promotes extensive reorganization of residual neural pathways that improves locomotion with and even without stimulation[21,25,26].

Here, we report the development of targeted neurotechnologies for delivering spatiotemporal EES during overground locomotor training with a gravity-assist device in humans[27]. We hypothesized that spatiotemporal EES would immediately enable voluntary locomotion despite chronic paralysis, and that the ability to sustain active movements during training would promote meaningful functional improvements with and even without stimulation.

Targeted neurotechnologies and surgery

We developed a wireless environment that allows real-time control over independently adjusted EES trains to the spinal cord during overground

[1]Center for Neuroprosthetics and Brain Mind Institute, School of Life Sciences, Swiss Federal Institute of Technology (EPFL), Lausanne, Switzerland. [2]Department of Clinical Neuroscience, Lausanne University Hospital (CHUV), Lausanne, Switzerland. [3]Platform of Translational Neuroscience, Department of Neuroscience and Movement Science, University of Fribourg, Fribourg, Switzerland. [4]GTXmedical, Lausanne, Switzerland. [5]Institute of Bioengineering, Swiss Federal Institute of Technology (EPFL), Lausanne, Switzerland. [6]Department of Radiology and Medical Informatics, University of Geneva, Geneva, Switzerland. [7]Department of Neurosurgery, Lausanne University Hospital (CHUV), Lausanne, Switzerland. [8]Department of Diagnostic and Interventional Radiology, Lausanne University Hospital (CHUV), Lausanne, Switzerland. [9]Department of Nuclear Medicine and Molecular Imaging, Lausanne University Hospital (CHUV), Lausanne, Switzerland. [10]Medtronic, Minneapolis, MN, USA. [11]Foundation for Research on Information Technologies in Society (IT'IS), Zurich, Switzerland. [12]Department for Information Technology and Electrical Engineering, Swiss Federal Institute of Technology (ETHZ), Zurich, Switzerland. [13]Department of Engineering Science, University of Oxford, Oxford, UK. [14]Faculty of Biology and Medicine, University of Lausanne (UNIL), Lausanne, Switzerland. [15]These authors contributed equally: Fabien B. Wagner, Jean-Baptiste Mignardot, Camille G. Le Goff-Mignardot. [16]These authors jointly supervised this work: Karen Minassian, Jocelyne Bloch, Grégoire Courtine. *e-mail: gregoire.courtine@epfl.ch

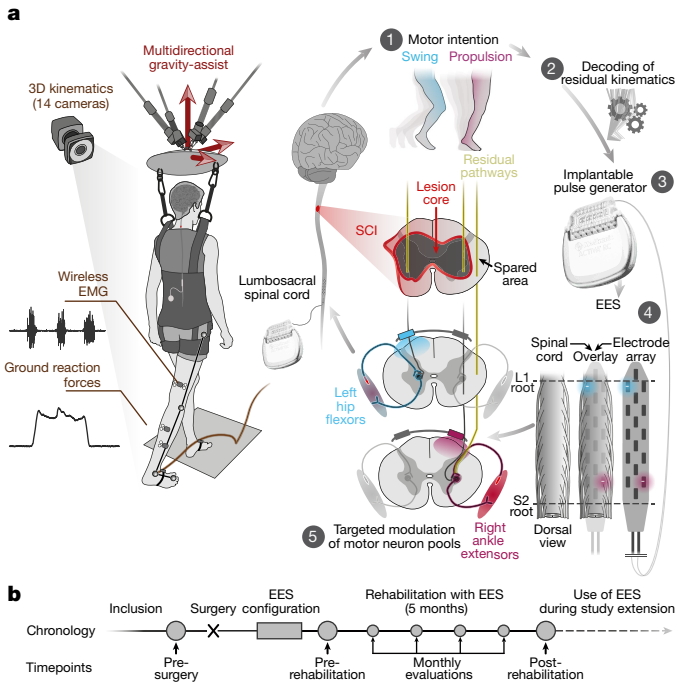

Fig. 1 | Technology and study design. a, Targeted neurotechnologies enable walking after SCI. Multidirectional assistance of trunk movements during overground locomotion while 3D kinematics, ground reaction forces and EMG activity are recorded wirelessly. An implantable pulse generator connected to a 16-electrode paddle array was used to target the posterior roots projecting to specific motor neuron pools, illustrated for hip flexors and ankle extensors. Real-time processing of residual kinematics ensures that targeted EES coincides with movement intent. **b**, Study timeline.

walking (Fig. 1a and Supplementary Video 1). A gravity-assist applied multidirectional forces to the trunk to provide personalized bodyweight support in a safe workspace[27]. A recording platform allowed real-time processing of whole-body kinematics, ground reaction forces and electromyographic (EMG) activity of leg muscles. To deliver stimulation, we upgraded an implantable pulse generator commonly used for deep brain stimulation with wireless communication modules[23] that enabled real-time control over EES parameters (Extended Data Fig. 1). EES sequences could be pre-programmed in an open loop or triggered in a closed loop on the basis of external signals[21,22]. The lumbosacral posterior roots were targeted using a 16-electrode paddle array designed for pain therapy.

We enrolled three males with a chronic cervical SCI who displayed severe lower limb deficits or complete paralysis that prevented them from walking overground (Extended Data Table 1).

To target the posterior roots that project to motor neuron pools that innervate leg muscles (Fig. 2a), we developed a surgical protocol consisting of pre-operative imaging combined with intraoperative electrophysiology and radiology that guided the precise placement of the paddle array (Extended Data Fig. 1b).

EES enables control of paralysed muscles

We aimed to identify electrode configurations that target the posterior roots that project to spinal cord regions, containing motor neurons involved in mobilizing the hip, knee and ankle joints.

We compiled an atlas of motor neuron activation maps underlying flexion or extension of each joint in healthy individuals. We projected the EMG activity from leg muscles onto the expected anatomical locations of the associated motor neuron pools[28,29]. We obtained consistent motor neuron activation maps. For example, hip flexion involved the activation of upper lumbar segments, whereas ankle extension activated motor neuron pools restricted to upper sacral segments (Fig. 2b).

To identify electrodes that could target the posterior roots that project to the spinal cord regions associated with these motor neuron activation maps, we performed simulations using hybrid computational models of EES[18]. Each model was personalized using magnetic resonance imaging (MRI) and computerized tomography (CT) scans. Simulations estimated the relative recruitment of each posterior root by each electrode of the array (Fig. 2c).

These simulations guided the identification of optimal electrode configurations. While participants laid supine, we delivered monopolar pulses of EES at increasing intensities through the electrodes that had the highest probabilities of activating the targeted posterior roots (Extended Data Fig. 2). Projection of muscle response amplitudes into circular plots described the spatial selectivity of each electrode, which we quantified with an algorithm (Fig. 2d). If the selectivity was insufficient, we steered the electrical field with multipolar electrode configurations (Extended Data Fig. 2).

For all participants, computer simulations and electrophysiological experiments confirmed high correlations between the identified electrode configurations and the recruitment of the posterior roots that project to each of the targeted spinal cord regions involved in mobilizing hip, knee and ankle joints (Extended Data Fig. 3).

We next tested whether spatially selective EES could facilitate force production from the targeted muscles. While seated, participants were asked to produce an isometric force restricted to a single joint. Participant 1 (P1) failed to produce hip flexion and ankle extension torques with his paralysed leg (Fig. 2e, f). EES immediately enabled voluntary activation of the targeted muscles to produce the desired torque. These observations were repeated for all targeted joints and participants (Extended Data Fig. 4).

Without any voluntary contribution, EES induced minimal muscle contraction (Extended Data Fig. 4). At the amplitudes used, EES augmented the excitability of the targeted motor neurons, which enabled residual but functionally silent descending inputs to activate muscles.

EES modulates cortical activity

These results opened the possibility that the recruitment of proprioceptive pathways with EES modulates cortical excitability, which may facilitate movement[30].

To study this hypothesis, we recorded electroencephalographic (EEG) activity when participants attempted to produce knee extension torques without and with EES (Extended Data Fig. 5a). EES triggered a robust response in the sensorimotor cortex (latency: 90–140 ms, Extended Data Fig. 5b), probably resulting from the recruitment of proprioceptive afferents.

Attempts to activate knee extensor muscles triggered event-related desynchronization (ERD) of the contralateral sensorimotor cortex in β-band frequencies, both without and with EES. This cortical activity has been linked to movement execution, and is followed by event-related resynchronization (ERS) after movement termination[31]. Previous studies showed that the amplitude of ERS decreases in proportion to severity of SCI[31]. Voluntary activation of paralysed muscles during EES led to an increase in ERS amplitude (Extended Data Fig. 5c, d). These results suggest that EES enhances cortical excitability, promoting more natural dynamics during movement execution[30].

Spatiotemporal EES enables walking

Walking involves reproducible sequences of muscle activation (Fig. 3a). The underlying motor neuron activation maps involve a succession of hotspots for which the migration reflects body mechanics[28], ensuring weight acceptance, propulsion and swing (Fig. 3b).

Targeted EES effectively activated the regions embedding these hotspots (Fig. 3c). To configure EES sequences (Fig. 3d, e), we fine-tuned the timing of each spatially selective stimulation train using a closed-loop controller that triggered EES on the basis of foot trajectory[21,22,32]. We adjusted the onset and duration of each train to approach the motor neuron activation maps of healthy individuals (Extended Data Fig. 6). Relatively small changes in the timing of each train altered performance (Extended Data Fig. 6b). Once optimized, EES could be delivered in an open loop: participants regulated the timing of their movements

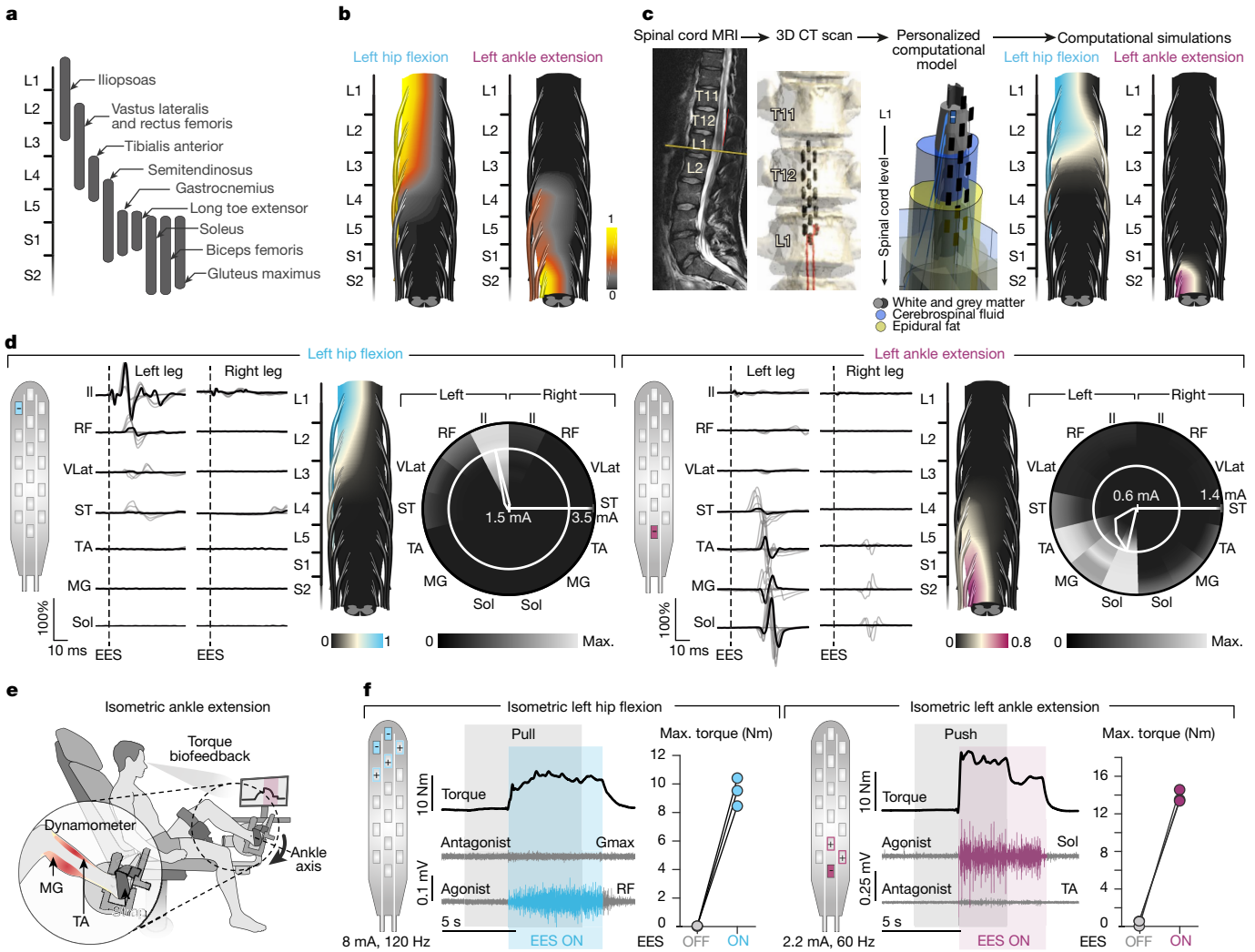

Fig. 2 | Configuration of targeted EES. a, Distribution of motor neuron pools within the spinal cord[46]. **b**, Map of motor neuron activation underlying isometric torque production in a healthy subject (consistent across three repetitions and subjects). **c**, Personalized computational model of EES. Simulated map of motor neuron activation following EES targeting the L1 and S2 posterior roots. **d**, Electrophysiological experiments were used to determine optimal electrodes and amplitudes for targeting specific spinal cord regions. EMG responses when delivering single-pulse EES at increasing amplitudes are shown (grey traces). Motor neuron activation maps correspond to optimal amplitudes (black traces). Circular plots report EMG amplitude (in grey scale) at increasing amplitudes (radial axis). White circles show optimal amplitudes; polygons quantify selectivity at this amplitude. **e**, Instrumented chair used to measure single-joint torques. **f**, Targeted EES enables voluntary force production by paralysed muscles. Isometric torque and EMG activity while delivering targeted EES, including quantification ($n = 3$ repetitions, P1). Gmax, gluteus maximus; Il, iliopsoas; MG, medial gastrocnemius; RF, rectus femoris; Sol, soleus; ST, semitendinosus; TA, tibialis anterior; VLat, vastus lateralis.

to pre-programmed EES sequences, which improved gait consistency (Extended Data Fig. 6c).

To tune muscle activity, we adjusted EES amplitudes and frequencies (Extended Data Fig. 6). As observed in animal models[21,22], we found a monotonic relationship between EES frequency and flexor muscle activity (Fig. 3f), such that increasing frequency proportionally enhanced flexion (Extended Data Fig. 6d). Unexpectedly, extensor motor neuron pools responded inversely. Proprioceptive afferents elicit strong monosynaptic responses in extensor motor neurons, whereas these afferents primarily engage flexor motor neurons through polysynaptic circuits[33]. In humans, monosynaptic projections are highly sensitive to low-frequency depression[34], which may explain the decrease in extensor motor neuron activation with increasing frequency.

Within five days, this procedure led to EES sequences (Fig. 3d, e) that enabled robust EMG activity in otherwise quiescent muscles during stepping on a treadmill (Extended Data Fig. 7).

Participants were then asked to walk overground using the gravity-assist and spatiotemporal EES. The stimulation enabled all participants to walk voluntarily until the stimulation was stopped. They could resume locomotion as soon as the stimulation was reintroduced (Fig. 4a, Extended Data Fig. 8a and Supplementary Video 2).

We next investigated participants' ability to adjust leg movements. First, we asked them to produce exaggerated step elevations without changing EES parameters. All participants were able to enhance their step elevation three-to-fivefold compared to regular steps (Fig. 4b and Extended Data Fig. 8b). Second, we asked them to adjust their stride to varying speeds. Not only were the participants able to adjust their stride length, but they also could stop locomotor movements despite the treadmill belt motion and ongoing stimulation (Extended Data Fig. 8b, e).

Finally, we asked participants to walk on a treadmill for one hour. All participants sustained more than 1,200 steps, covering distances as long as 1.0 km without showing muscle exhaustion or gait impairments (Fig. 4c and Extended Data Fig. 8c).

These results show that spatiotemporal EES not only enabled completely or partially paralysed individuals to walk overground, but also allowed them to adjust leg movements to stand and walk over a range of speeds for durations as long as one hour.

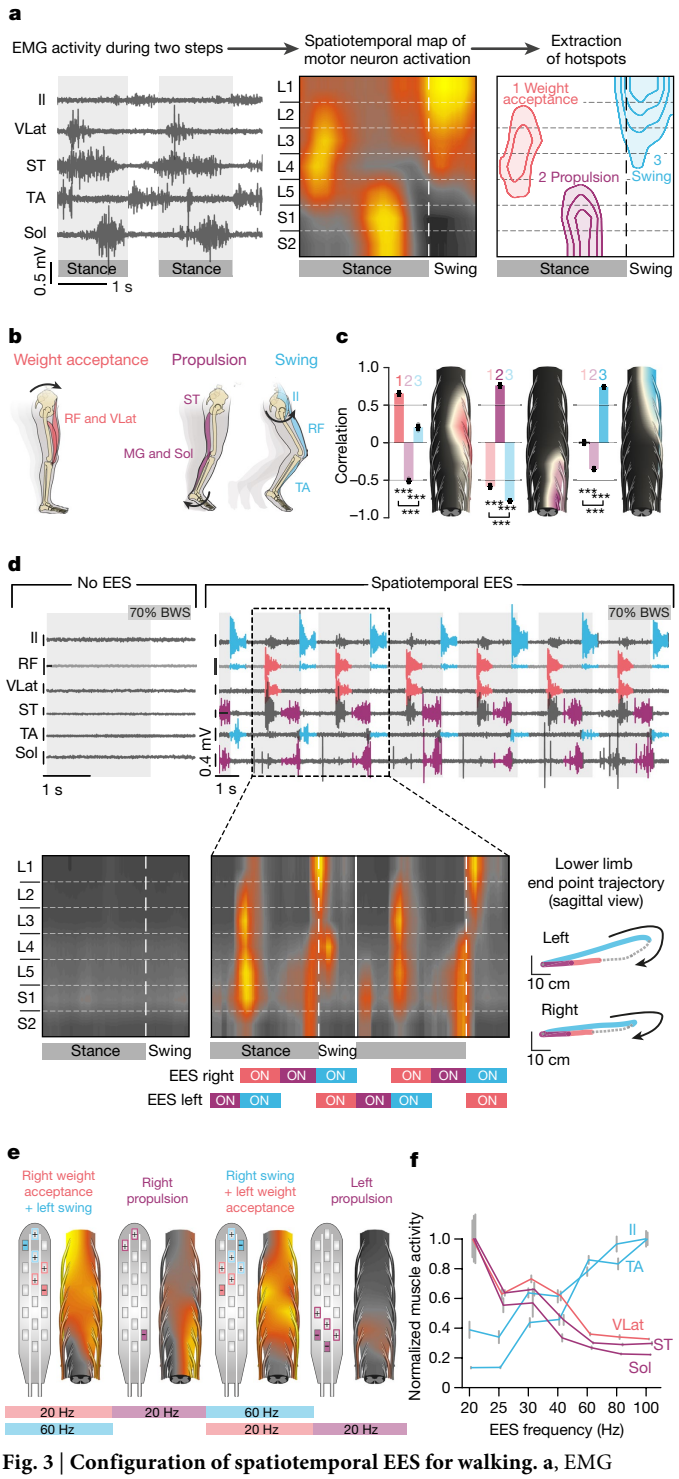

Fig. 3 | Configuration of spatiotemporal EES for walking. a, EMG activity during walking in healthy individuals. Spatiotemporal map of motor neuron activation highlights hotspots (mean, $n = 12$ gait cycles, representative subject). Equipotential lines represent 45–75% activation. **b**, Functional target of each hotspot. **c**, Map of motor neuron activation following 500-ms bursts of targeted EES during standing. Bar plots show Pearson's correlations for each hotspot (mean ± s.e.m., $n = 12$ bursts, $^{***}P < 0.001$; one-way ANOVA, post hoc Tukey's honest significant difference (HSD) test). **d**, EMG activity and map of motor neuron activation during EES or without EES after a motor complete SCI while stepping on a treadmill with support and assistance (P3). EES timing is indicated along foot trajectories (bottom right; $n = 73$ steps) and below motor neuron activation maps. **e**, Spatiotemporal EES sequence for data shown in **d**. **f**, Mean (± s.e.m.) modulation of EMG amplitude in flexor and extensor muscles during walking with increasing EES frequencies ($n = 20, 15, 16, 17, 15, 16, 15$ gait cycles for 20, 25, 30, 40, 60, 80, 100 Hz, respectively; P3).

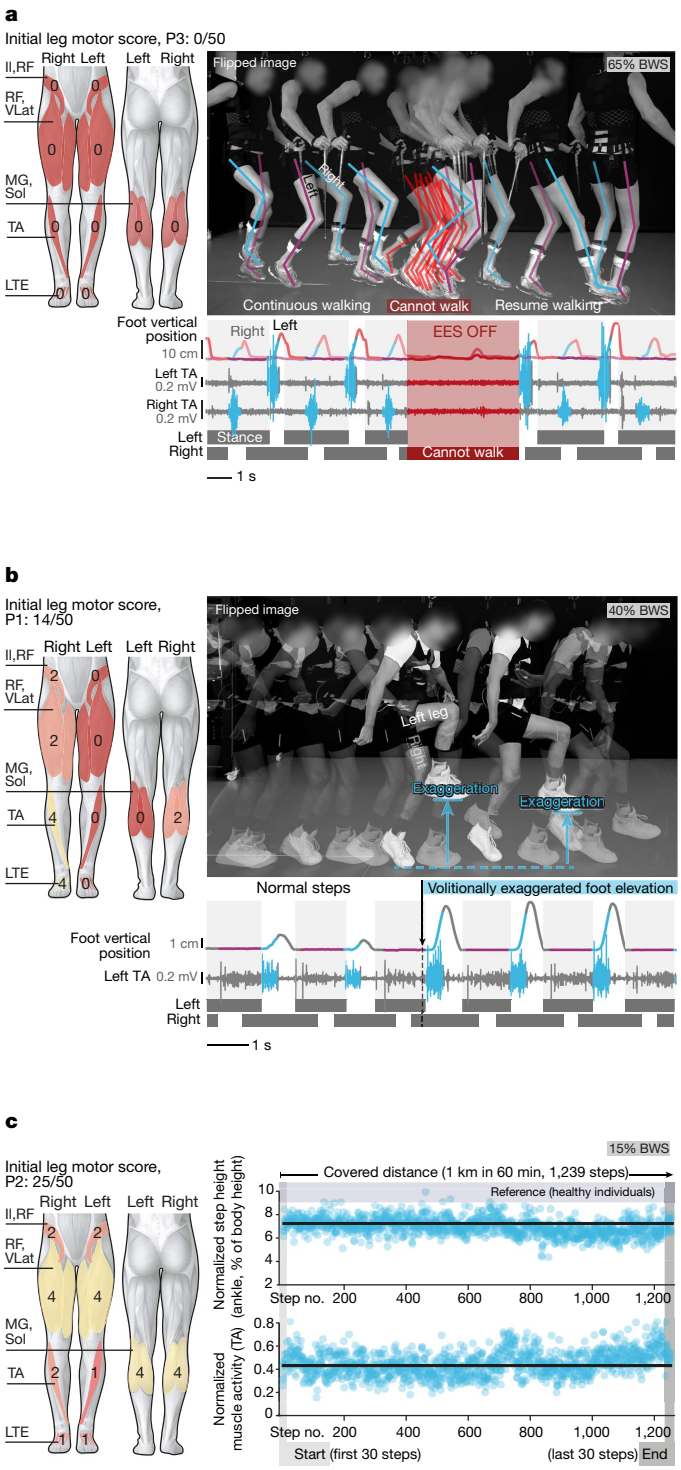

Fig. 4 | Voluntary control of adaptive and sustained locomotion. a, Spatiotemporal EES enables voluntary control of overground walking. Chronophotography, tibialis anterior (TA) EMG activity and foot vertical position during overground walking with gravity-assist and sticks while EES is switched on, then off, then on. Leg motor scores shown on muscles in diagrams: 0, total paralysis; 1, palpable or visible contraction; 2, active movement, gravity eliminated; 3, active movement against gravity; 4, active movement against some resistance; 5, active movement against full resistance. **b**, Spatiotemporal EES enables voluntary control of leg kinematics. Overground walking when participants were requested to perform steps with normal heights and then exaggerated step elevations. **c**, Spatiotemporal EES enables sustained walking. Consecutive values of step height and EMG activity over 60 min of walking with EES (P1: 1.2 km; P2, P3: 1 km). Experiments in **a**, **b** were repeated at least five times; the experiment in **c** was performed once, but participants routinely walked for 60 min during training. BWS, bodyweight support.

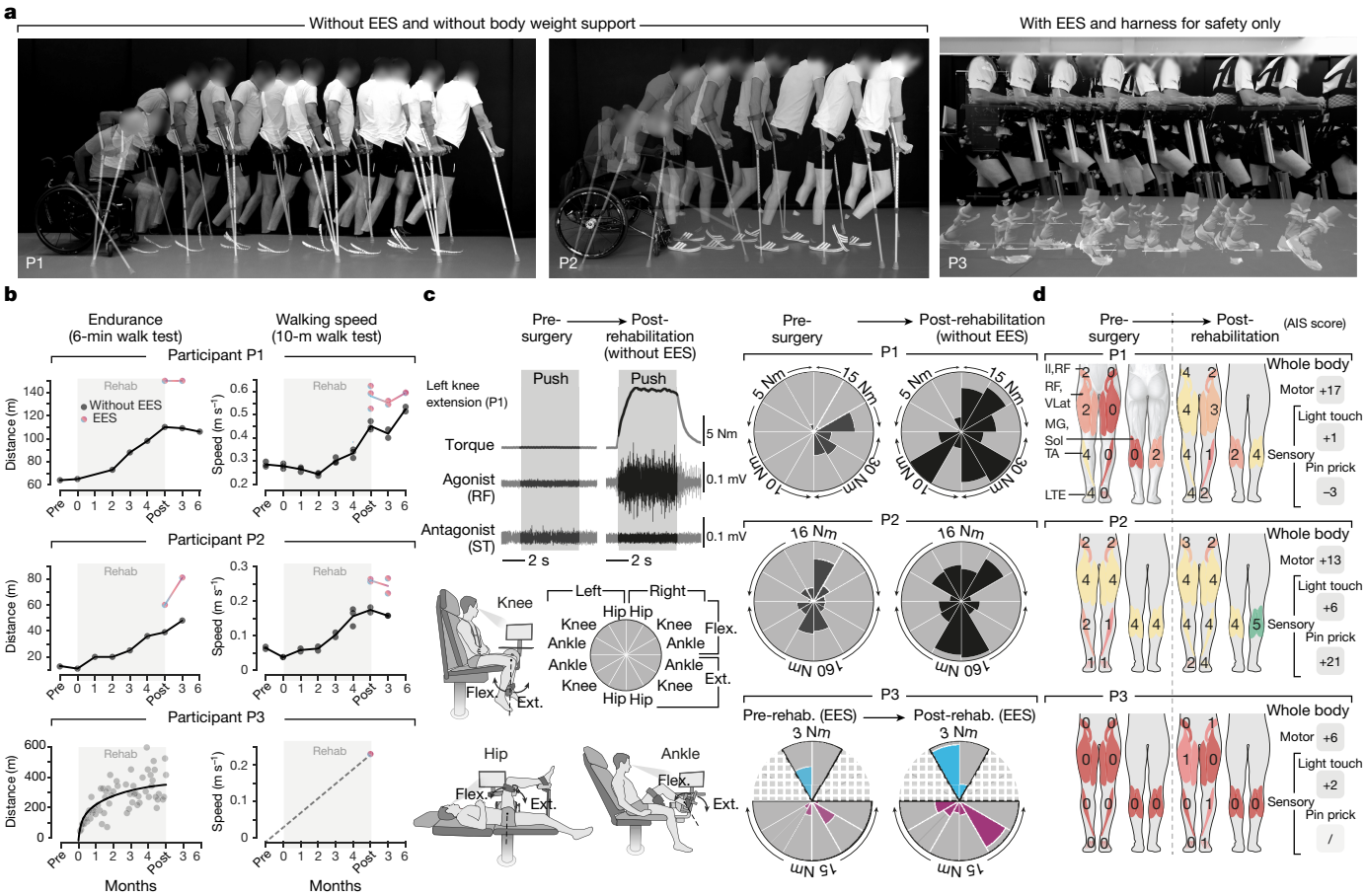

Fig. 5 | Rehabilitation mediates neurological recovery. a, Improved mobility after rehabilitation. Chronophotography shows P1 and P2 transiting from sitting to walking with crutches without EES; P3 progresses overground with a walker and EES; repeated at least three times on different days. **b**, Plots reporting changes in 6-min and 10-m walk tests for P1 and P2. Tests were performed without gravity-assist, following clinical guidance. For P3 plots report changes in walking distance during rehabilitation and walking speed with EES (with transparent body weight support). **c**, Evaluations of isometric torque production for each joint, quantified before surgery and after rehabilitation without EES for P1 and P2, and with EES for P3. **d**, Changes in lower limb motor and sensory scores after rehabilitation. Changes in motor and sensory scores on abbreviated injury scale (AIS) for all levels below injury are summarized (see Extended Data Table 1).

Continuous EES is poorly effective

Recent studies have shown that continuous EES enabled overground walking after nearly one year of intense training[9,10]. As spatiotemporal EES enabled locomotion within one week, we evaluated whether continuous EES could achieve similar efficacy.

We delivered widespread stimulation targeting the posterior roots associated with flexor motor neuron pools, as previously recommended[10]. However, we did not further optimize the stimulation. Continuous EES enhanced muscle activity, but was poorly effective in facilitating locomotion overground. All participants reported a loss of limb position awareness combined with co-activation across muscles (Extended Data Fig. 9 and Supplementary Video 3). These detrimental outcomes are due to the cancellation of proprioceptive information during continuous EES[35].

Rehabilitation improves walking with EES

Participants followed a rehabilitation program four to five times per week for five months (Fig. 1b), focused on walking on a treadmill and overground; this was complemented with muscle strengthening and standing, each of which was enabled by task-specific EES (Extended Data Fig. 10a).

With spatiotemporal EES, all participants improved their walking capacities following a reproducible chronology (Extended Data Fig. 10b): non-ambulatory participants initially required crutches and the gravity-assist to walk overground. After one to three months, they could walk hands-free when provided with hip support in the gravity-assist. Eventually, P1 and P2 regained independent walking while 35% of their bodyweight was supported against gravity. P3 needed a walker to progress overground with EES (Supplementary Video 4).

Neurological recovery without EES

Improvements were not limited to walking with EES. Rehabilitation promoted neurological recovery that translated into improvements without EES.

P1 and P2 could transit from sitting to standing and walking independently with crutches (Fig. 5a). P1 could even walk without an assistive device for several steps (Supplementary Video 5). Consequently, P1 and P2 increased their WISCI (walking index for spinal cord injury) scores from 13 to 16 and 6 to 13, respectively. They displayed substantial improvements in clinical evaluations such as ten-metre and six-minute walking tests without EES (Fig. 5b). Several months after completing the rehabilitation program, both participants, who continued practicing once or twice per week with EES, maintained or further improved their performance.

Participants also recovered voluntary leg movements without EES. For example, P1 and P3 could sustain a full extension of their previously paralysed legs against gravity (P3, lying only; Extended Data Fig. 11c and Supplementary Video 5). Quantified measurements revealed that P1 and P2 improved their ability to produce a torque at each joint of

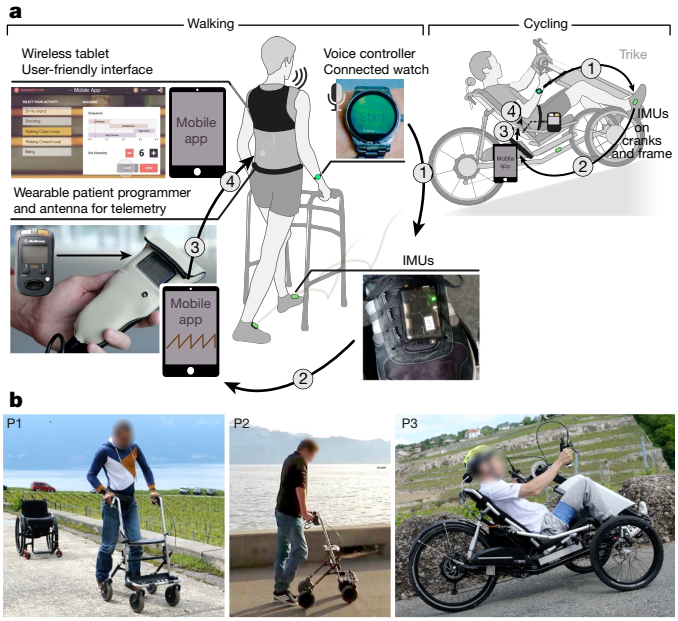

Fig. 6 | Spatiotemporal EES in ecological settings. a, System to support activities of daily living. Tablet featuring a mobile App allows participants to select EES sequences, delivered in open loop or closed loop based on inertial measurement units (IMUs) located on both feet or attached onto the cranks and frame of a trike. 1. A personalized voice-controlled watch allows the user to switch EES on or off. 2. IMUs detect foot or crank motion during walking or cycling. 3. Controller sends commands to the patient programmer. 4. Spatiotemporal EES is adjusted in a closed loop. **b**, Walking and cycling activities in ecological settings are enabled by spatiotemporal EES.

both legs (Fig. 5c). This recovery translated into an increase of 16 and 11 points in lower extremity motor scores, respectively (Fig. 5d). Both participants had previously followed extensive conventional rehabilitation without showing neurological recovery. The lower extremity motor score increased by 4 points in participant P3, but without EES this recovery was insufficient to produce measurable forces when seated. However, force production improved during EES (Fig. 5c). He showed a considerable increase in mass and quality of thigh and trunk muscles (Extended Data Fig. 11). P1, P2 and P3 also showed improvements in upper limb motor scores of 1, 2 and 2 points, respectively.

Support of activities in the community

Recovery of functional leg movements during spatiotemporal EES suggested that practical stimulation technologies could support activities of daily living. For this purpose, we engineered a solution based on a tablet to enable the selection of EES sequences that are switched on or off with a voice-controlled watch (Fig. 6a). To enable standing, walking or cycling, EES sequences must be synchronized to the intended movements. We conceived algorithms that trigger and adjust the timing of EES trains in a closed loop based on real-time acquisition of signals from wearable inertial measurement units.

Robust event-triggered detection allowed participants to transit from sitting to standing and walking freely in ecological settings (Fig. 6b and Extended Data Fig. 12). A stimulation program specific for cycling permitted participants to ride an adapted trike powered with the arms and legs (Supplementary Video 6).

Discussion

We developed targeted EES neurotechnologies that immediately restored voluntary control of walking in individuals with severe or complete paralysis. The electrode configurations targeted proprioceptive circuits through the recruitment of selected posterior roots[17–19,36]. This strategy was pivotal to enable the immediate control of walking despite chronic paralysis. This framework guided the rapid personalization of spatiotemporal EES sequences that continuously coincided with intended movements. Consequently, EES augmented the excitability of motor neuron pools that were concomitantly engaged by the natural flow of sensory information and residual supraspinal commands. This spatiotemporal convergence enabled more robust and natural control of leg movements compared to empirical stimulation paradigms such as continuous EES[9,10].

We hypothesize that this spatiotemporal convergence is responsible for the neurological recovery observed in all participants without EES. We showed that mice lacking proprioceptive circuits exhibit defective rearrangement of descending pathways after SCI, which abolishes recovery[37]. Conversely, we propose that the spatiotemporal contingence between residual supraspinal commands and proprioceptive circuit activations with EES may increase the strength and number of terminals from spared descending projections through bidirectional spike-timing-dependent plasticity[38,39]. Electrophysiological studies have documented such plasticity in humans with SCI[40,41]. This interpretation is consistent with the pronounced reorganization of cortico-reticulo-spinal circuits observed in rodents when EES enables gait training despite paralysis[25,26]. As we observed in humans, rodents regained cortical control of leg movements that persisted without EES[25] when rehabilitation commenced early after SCI. We therefore anticipate that this therapy will be even more efficacious early after SCI in humans, when the potential for plasticity is elevated and the neuromuscular system has not yet undergone the atrophy that follows chronic paralysis[42]. Furthermore, improvements in muscle mass and other physiological functions[43,44] suggest that EES may help to counteract these deteriorations.

Clinical trials starting early after SCI will require a stratification of participants who may benefit from the therapy, combined with statistical models that predict their potential for recovery[45]. Here, we validated our neurotechnologies in a few individuals. This proof-of-concept stresses the urgency of developing neurotechnologies that not only harness targeted EES to enable movement, but also provide the usability features to support rehabilitation in clinical settings and use in the community.

Data availability

Data that support the findings and software routines developed for the data analysis will be made available upon reasonable request to the corresponding author.

Online content

Any methods, additional references, Nature Research reporting summaries, source data, statements of data availability and associated accession codes are available at https://doi.org/10.1038/s41586-018-0649-2.

Received: 22 June 2018; Accepted: 1 October 2018;
Published online 31 October 2018.

1. Behrman, A. L., Ardolino, E. M. & Harkema, S. J. Activity-based therapy: from basic science to clinical application for recovery after spinal cord injury. *J. Neurol. Phys. Ther.* **41**, S39–S45 (2017).
2. Jones, M. L. et al. Activity-based therapy for recovery of walking in individuals with chronic spinal cord injury: results from a randomized clinical trial. *Arch. Phys. Med. Rehabil.* **95**, 2239–2246 (2014).
3. Field-Fote, E. C., Lindley, S. D. & Sherman, A. L. Locomotor training approaches for individuals with spinal cord injury: a preliminary report of walking-related outcomes. *J. Neurol. Phys. Ther.* **29**, 127–137 (2005).
4. Edgerton, V. R. et al. Training locomotor networks. *Brain Res. Rev.* **57**, 241–254 (2008).
5. Côté, M. P., Murray, M. & Lemay, M. A. Rehabilitation strategies after spinal cord injury: inquiry into the mechanisms of success and failure. *J. Neurotrauma* **34**, 1841–1857 (2017).
6. Borton, D., Micera, S., Millán, J. d. R. & Courtine, G. Personalized neuroprosthetics. *Sci. Transl. Med.* **5**, 210rv2 (2013).
7. Field-Fote, E. C. & Roach, K. E. Influence of a locomotor training approach on walking speed and distance in people with chronic spinal cord injury: a randomized clinical trial. *Phys. Ther.* **91**, 48–60 (2011).
8. Minassian, K., McKay, W. B., Binder, H. & Hofstoetter, U. S. Targeting lumbar spinal neural circuitry by epidural stimulation to restore motor function after spinal cord injury. *Neurotherapeutics* **13**, 284–294 (2016).
9. Angeli, C. A. et al. Recovery of over-ground walking after chronic motor complete spinal cord injury. *N. Engl. J. Med.* **379**, 1244–1250 (2018).

10. Gill, M. L. et al. Neuromodulation of lumbosacral spinal networks enables independent stepping after complete paraplegia. *Nat. Med.* https://doi.org/10.1038/s41591-018-0175-7 (2018).
11. Barolat, G., Myklebust, J. B. & Wenninger, W. Enhancement of voluntary motor function following spinal cord stimulation-case study. *Appl. Neurophysiol.* **49**, 307–314 (1986).
12. Angeli, C. A., Edgerton, V. R., Gerasimenko, Y. P. & Harkema, S. J. Altering spinal cord excitability enables voluntary movements after chronic complete paralysis in humans. *Brain* **137**, 1394–1409 (2014).
13. Danner, S. M. et al. Human spinal locomotor control is based on flexibly organized burst generators. *Brain* **138**, 577–588 (2015).
14. Grahn, P. J. et al. Enabling task-specific volitional motor functions via spinal cord neuromodulation in a human with paraplegia. *Mayo Clin. Proc.* **92**, 544–554 (2017).
15. Carhart, M. R., He, J., Herman, R., D'Luzansky, S. & Willis, W. T. Epidural spinal-cord stimulation facilitates recovery of functional walking following incomplete spinal-cord injury. *IEEE Trans. Neural Syst. Rehabil. Eng.* **12**, 32–42 (2004).
16. Minassian, K. et al. Stepping-like movements in humans with complete spinal cord injury induced by epidural stimulation of the lumbar cord: electromyographic study of compound muscle action potentials. *Spinal Cord* **42**, 401–416 (2004).
17. Rattay, F., Minassian, K. & Dimitrijevic, M. R. Epidural electrical stimulation of posterior structures of the human lumbosacral cord: 2. Quantitative analysis by computer modeling. *Spinal Cord* **38**, 473–489 (2000).
18. Capogrosso, M. et al. A computational model for epidural electrical stimulation of spinal sensorimotor circuits. *J. Neurosci.* **33**, 19326–19340 (2013).
19. Moraud, E. M. et al. Closed-loop control of trunk posture improves locomotion through the regulation of leg proprioceptive feedback after spinal cord injury. *Sci. Rep.* **8**, 76 (2018).
20. Gerasimenko, Y., Roy, R. R. & Edgerton, V. R. Epidural stimulation: comparison of the spinal circuits that generate and control locomotion in rats, cats and humans. *Exp. Neurol.* **209**, 417–425 (2008).
21. Wenger, N. et al. Spatiotemporal neuromodulation therapies engaging muscle synergies improve motor control after spinal cord injury. *Nat. Med.* **22**, 138–145 (2016).
22. Wenger, N. et al. Closed-loop neuromodulation of spinal sensorimotor circuits controls refined locomotion after complete spinal cord injury. *Sci. Transl. Med.* **6**, 255ra133 (2014).
23. Capogrosso, M. et al. A brain-spine interface alleviating gait deficits after spinal cord injury in primates. *Nature* **539**, 284–288 (2016).
24. Dominici, N. et al. Versatile robotic interface to evaluate, enable and train locomotion and balance after neuromotor disorders. *Nat. Med.* **18**, 1142–1147 (2012).
25. Asboth, L. et al. Cortico-reticulo-spinal circuit reorganization enables functional recovery after severe spinal cord contusion. *Nat. Neurosci.* **21**, 576–588 (2018).
26. van den Brand, R. et al. Restoring voluntary control of locomotion after paralyzing spinal cord injury. *Science* **336**, 1182–1185 (2012).
27. Mignardot, J. B. et al. A multidirectional gravity-assist algorithm that enhances locomotor control in patients with stroke or spinal cord injury. *Sci. Transl. Med.* **9**, eaah3621 (2017).
28. Cappellini, G., Ivanenko, Y. P., Dominici, N., Poppele, R. E. & Lacquaniti, F. Migration of motor pool activity in the spinal cord reflects body mechanics in human locomotion. *J. Neurophysiol.* **104**, 3064–3073 (2010).
29. Yakovenko, S., Mushahwar, V., VanderHorst, V., Holstege, G. & Prochazka, A. Spatiotemporal activation of lumbosacral motoneurons in the locomotor step cycle. *J. Neurophysiol.* **87**, 1542–1553 (2002).
30. Asanuma, H. & Mackel, R. Direct and indirect sensory input pathways to the motor cortex; its structure and function in relation to learning of motor skills. *Jpn. J. Physiol.* **39**, 1–19 (1989).
31. Gourab, K. & Schmit, B. D. Changes in movement-related β-band EEG signals in human spinal cord injury. *Clin. Neurophysiol.* **121**, 2017–2023 (2010).
32. Capogrosso, M. et al. Configuration of electrical spinal cord stimulation through real-time processing of gait kinematics. *Nat. Protoc.* **13**, 2031–2061 (2018).
33. Schieppati, M. The Hoffmann reflex: a means of assessing spinal reflex excitability and its descending control in man. *Prog. Neurobiol.* **28**, 345–376 (1987).
34. Schindler-Ivens, S. & Shields, R. K. Low-frequency depression of H-reflexes in humans with acute and chronic spinal-cord injury. *Exp. Brain Res.* **133**, 233–241 (2000).
35. Formento, E. et al. Electrical spinal cord stimulation must preserve proprioception to enable locomotion in humans with spinal cord injury. *Nat. Neurosci.* https://doi.org/10.1038/s41593-018-0262-6 (2018).
36. Moraud, E. M. et al. Mechanisms underlying the neuromodulation of spinal circuits for correcting gait and balance deficits after spinal cord injury. *Neuron* **89**, 814–828 (2016).
37. Takeoka, A., Vollenweider, I., Courtine, G. & Arber, S. Muscle spindle feedback directs locomotor recovery and circuit reorganization after spinal cord injury. *Cell* **159**, 1626–1639 (2014).
38. Holtmaat, A. & Svoboda, K. Experience-dependent structural synaptic plasticity in the mammalian brain. *Nat. Rev. Neurosci.* **10**, 647–658 (2009).
39. Nishimura, Y., Perlmutter, S. I., Eaton, R. W. & Fetz, E. E. Spike-timing-dependent plasticity in primate corticospinal connections induced during free behavior. *Neuron* **80**, 1301–1309 (2013).
40. Perez, M. A., Field-Fote, E. C. & Floeter, M. K. Patterned sensory stimulation induces plasticity in reciprocal Ia inhibition in humans. *J. Neurosci.* **23**, 2014–2018 (2003).
41. Urbin, M. A., Ozdemir, R. A., Tazoe, T. & Perez, M. A. Spike-timing-dependent plasticity in lower-limb motoneurons after human spinal cord injury. *J. Neurophysiol.* **118**, 2171–2180 (2017).
42. Dietz, V. Behavior of spinal neurons deprived of supraspinal input. *Nat. Rev. Neurol.* **6**, 167–174 (2010).
43. West, C. R. et al. Association of epidural stimulation with cardiovascular function in an individual with spinal cord injury. *JAMA Neurol.* **75**, 630–632 (2018).
44. Herrity, A. N., Williams, C. S., Angeli, C. A., Harkema, S. J. & Hubscher, C. H. Lumbosacral spinal cord epidural stimulation improves voiding function after human spinal cord injury. *Sci. Rep.* **8**, 8688 (2018).
45. van Middendorp, J. J. et al. A clinical prediction rule for ambulation outcomes after traumatic spinal cord injury: a longitudinal cohort study. *Lancet* **377**, 1004–1010 (2011).
46. Sharrard, W. J. The segmental innervation of the lower limb muscles in man. *Ann. R. Coll. Surg. Engl.* **35**, 106–122 (1964).

Acknowledgements See Supplementary Notes. Support: International Foundation for Research in Paraplegia (IRP), Wings for Life, Wyss Center for Neuroengineering, European Union's Horizon 2020 No.785907 (Human Brain Project SGA2), Eurostars No. E10889, GTXmedical, National Center of Competence in Research (NCCR) Robotics of the Swiss National Foundation, the Commission of Technology and Innovation Innosuisse (CTI) No. 25761.1, Voirol Foundation, Firmenich Foundation, Pictet Group Charitable Foundation, Panacée Foundation, riders4riders, SOFMER (to P.S.), the Whitaker International Scholars Program (to I.S.) and the H2020-MSCA-COFUND-2015 EPFL Fellows program (No. 665667 to F.B.W.).

Reviewer information *Nature* thanks C. Moritz, J. Henderson and K. Moxon for their contribution to the peer review of this work.

Author contributions N.B. and T.D., Neural Research Programmer development. F.B.W., Mi.C., C.G.L.G.-M., R.H., V.D. and J.v.Z., technological framework. J.B., surgeries. F.B.W., J.-B.M., C.G.L.G.-M., Ma.C., E.Pi., K.M., R.D., S.K., I.S. and G.C. performed and analysed experiments. R.D., S.K. and Ma.C. contributed equally. F.B., muscle data. I.F., L.M., M.V., P.S., I.S., F.B.W., J.-B.M., C.G.L.G.-M., K.M., K.V.D.K. and G.E., neurorehabilitation. K.V.D.K., F.B., J.P., B.S., E.Pr., P.S. and S.C., clinical and neurological evaluations. A.R. and Ma.C., computational framework. A.R., E.Pa., E.N. and N.K., computational simulations. J.-B.M., C.G.L.G.-M., R.D., S.K. and F.B.W. generated figures. A.W., M.V., R.B., V.D. and H.L., regulatory affairs. K.M., J.B. and G.C., conception and supervision. G.C. wrote the paper with J.B., F.B.W. and K.M.

Competing interests G.C., J.B., Ma.C. and V.D. hold various patents in relation to the present work. T.D., R.B. and N.B. are Medtronic employees, and V.D., H.L., J.v.Z., A.W., Mi.C. and E.Pa. are GTXmedical employees. In review of the manuscript they contributed to technical accuracy but did not influence the results or the content of the manuscript. G.C., J.B., V.D., and H.L. are founders and shareholders of GTXmedical, a company with direct relationships to the presented intervention.

Additional information

Extended data is available for this paper at https://doi.org/10.1038/s41586-018-0649-2.
Supplementary information is available for this paper at https://doi.org/10.1038/s41586-018-0649-2.

Correspondence and requests for materials should be addressed to G.C.

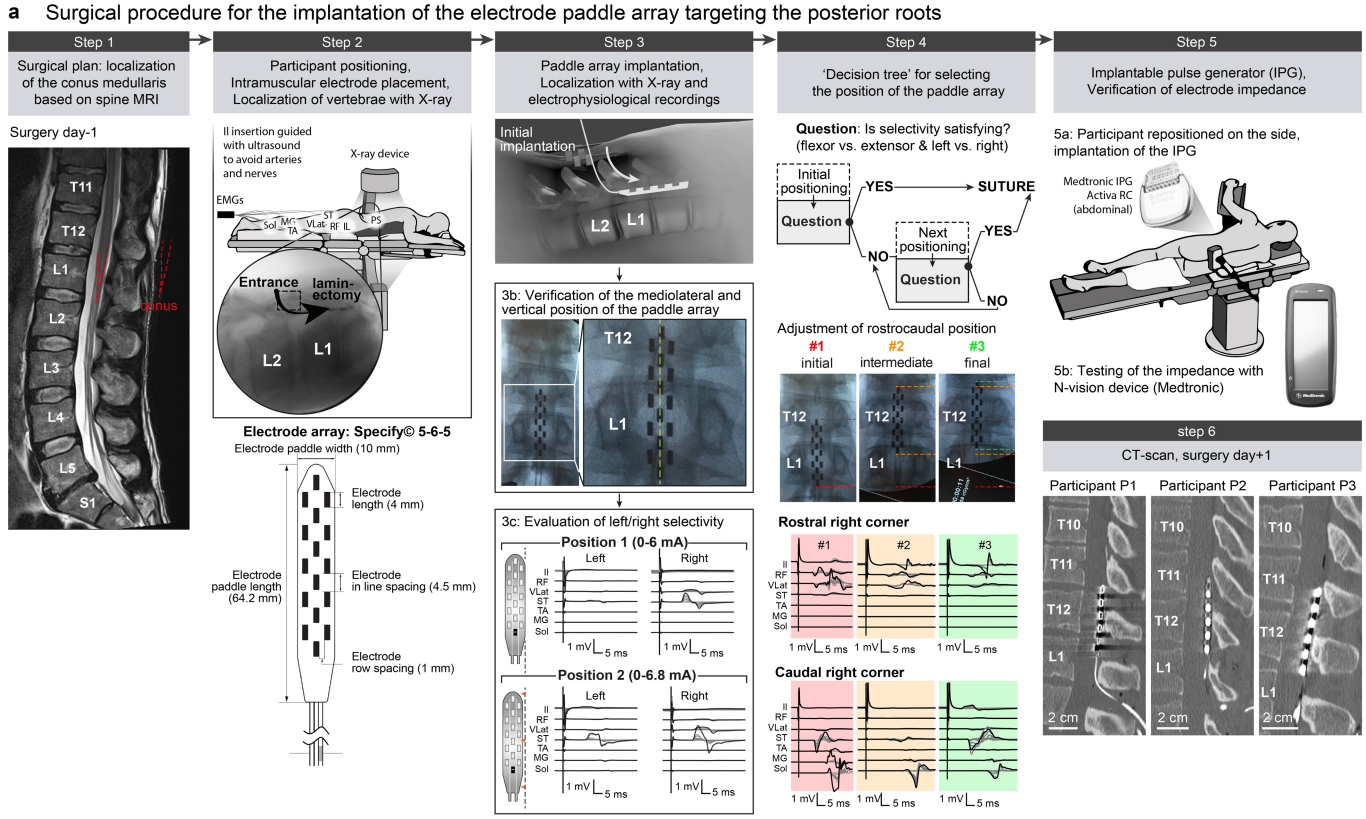

Extended Data Fig. 1 | Surgical procedure and technological framework. a, Surgery. Step 1: high-resolution MRI for pre-surgical planning. The entry point into the epidural space is based on the position of the conus. Step 2: placement of subdermal and intramuscular needle EMG electrodes for key leg muscles and paraspinal (PS) muscles. A subdermal needle is inserted over the sacrum and used as a return electrode for stimulation. Bottom, schematic of the 16-electrode paddle array. Step 3: surgical openings based on pre-surgical planning, typically between the L1 and L2 vertebrae, which are identified through intraoperative X-ray. The mediolateral positions of the paddle array are evaluated with X-ray and recordings of EMG responses following single pulses of EES delivered to the most rostral or most caudal midline electrodes. Step 4: the rostrocaudal position of the paddle array is optimized using EMG responses to single-pulse EES delivered to the electrodes located at each corner of the paddle array. The aim is to obtain strong ipsilateral responses in hip flexors with the most rostral electrodes and strong ipsilateral responses in ankle extensors with the most caudal electrodes. Step 5: implantable pulse generator (IPG) placed within the abdomen. Once connected to the paddle array, the impedance of the electrodes is evaluated to verify that all the components are properly connected. Step 6: post-surgical CT scan showing the location of the paddle array with respect to the vertebrae in each participant.
b, Technological framework and surgical procedure. Step 1: participants wear reflective markers that are monitored using infrared cameras. An algorithm assigns the markers to the joints in real-time. Step 2: the spatiotemporal trajectory of the foot around a calculated centre of rotation (centroid, updated every 3 s) is converted into angular coordinates that trigger and terminate EES protocols when a user-defined threshold is crossed. Step 3: EES commands are transmitted to the IPG via Bluetooth (1) to a module that converts them into infrared signals (2), which are then transferred to the stimulation programmer device (2′). Step 4: the stimulation programmer transmits EES commands into the IPG (4) via induction telemetry, using an antenna (3) taped to the skin and aligned to the IPG. EES is delivered through the paddle array (5).

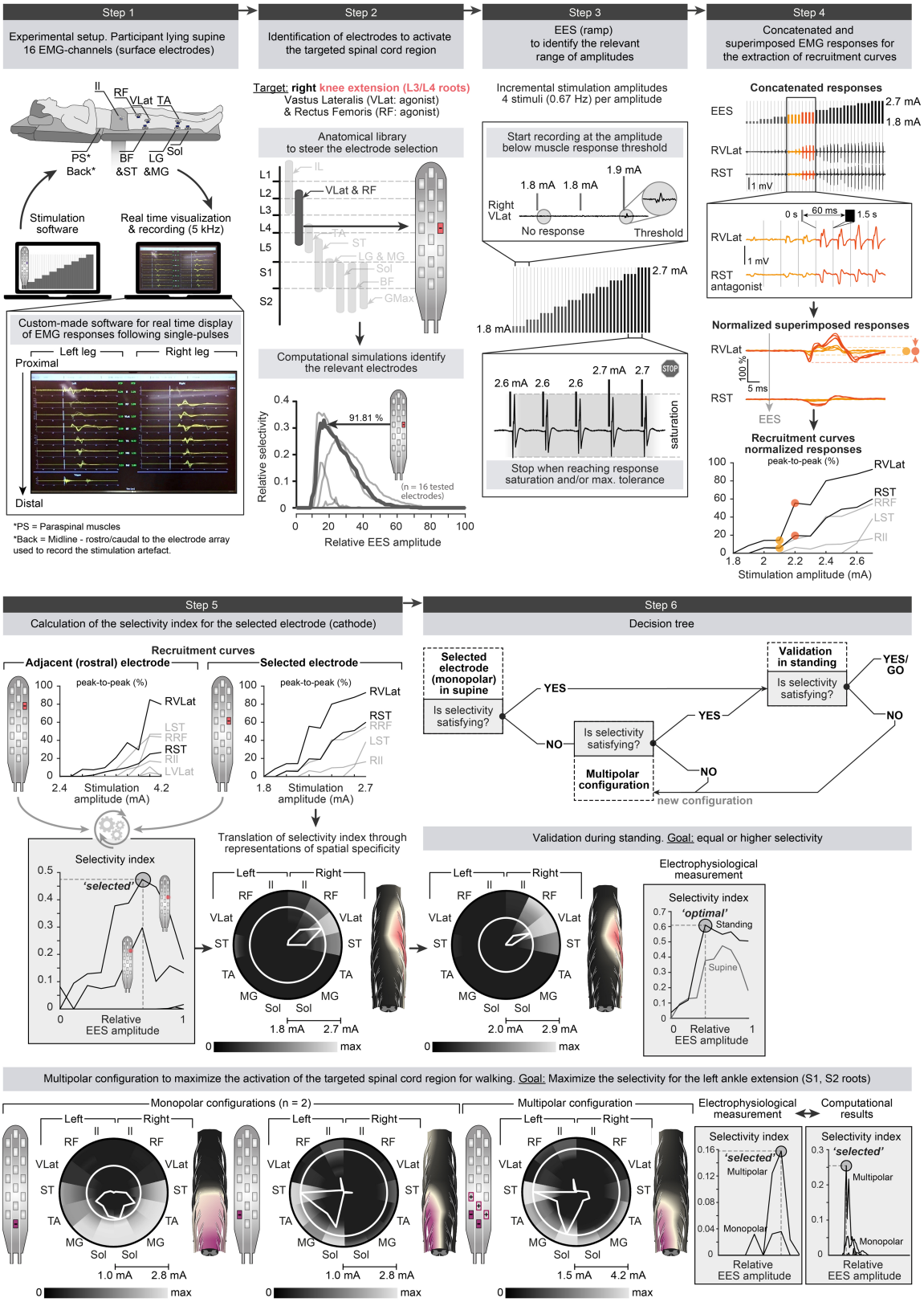

Extended Data Fig. 2 | See next page for caption.

Extended Data Fig. 2 | Identification of electrode configurations to target selected posterior roots. Step 1: single-pulse EES and EMG recording setup. Step 2: motor neuron pools are located in specific segments, which provides information on the relative recruitment of each posterior root with EES. For example, electrodes targeting the L3 or L4 posterior roots will elicit the strongest EMG responses in the knee extensors. A personalized computational model of EES allows the performance of simulations that evaluate the relative activation of a given posterior root with a given electrode over the entire amplitude range. Each curve corresponds to an electrode. The highlighted curve corresponds to the electrode selected after steps 3–5. Step 3: single pulses of EES are delivered through the subset of electrodes identified by simulations. The EMG responses are recorded over a broad range of EES amplitudes. Step 4: the EMG responses are concatenated and averaged across $n = 4$ repetitions for each EMG amplitude, and the peak-to-peak amplitude of the average responses is calculated to elaborate a recruitment curve for each recorded leg muscle (black traces: targeted muscles). Step 5: the circular plots display the normalized EMG responses (greyscale) when delivering single-pulse EES at increasing amplitudes (radial axis), where the white circle highlights the optimal EES amplitude and the polygon quantifies the relative muscular selectivity at this amplitude (median response taken over $n = 4$ EES pulses). The motor neuron activation maps are shown for the optimal amplitudes. Step 6: decision tree to validate or optimize electrode configurations. The selected electrode is tested during standing as the position of the spinal cord with respect to the paddle array can change between supine and standing. In this example, the selectivity improves during standing. When the selectivity is deemed insufficient, the current is steered towards the targeted posterior roots using multipolar configurations. The example shows the increased selectivity of a multipolar configuration with two cathodes surrounded by three anodes, compared to the two corresponding monopolar configurations. These results were verified experimentally and with computer simulations.

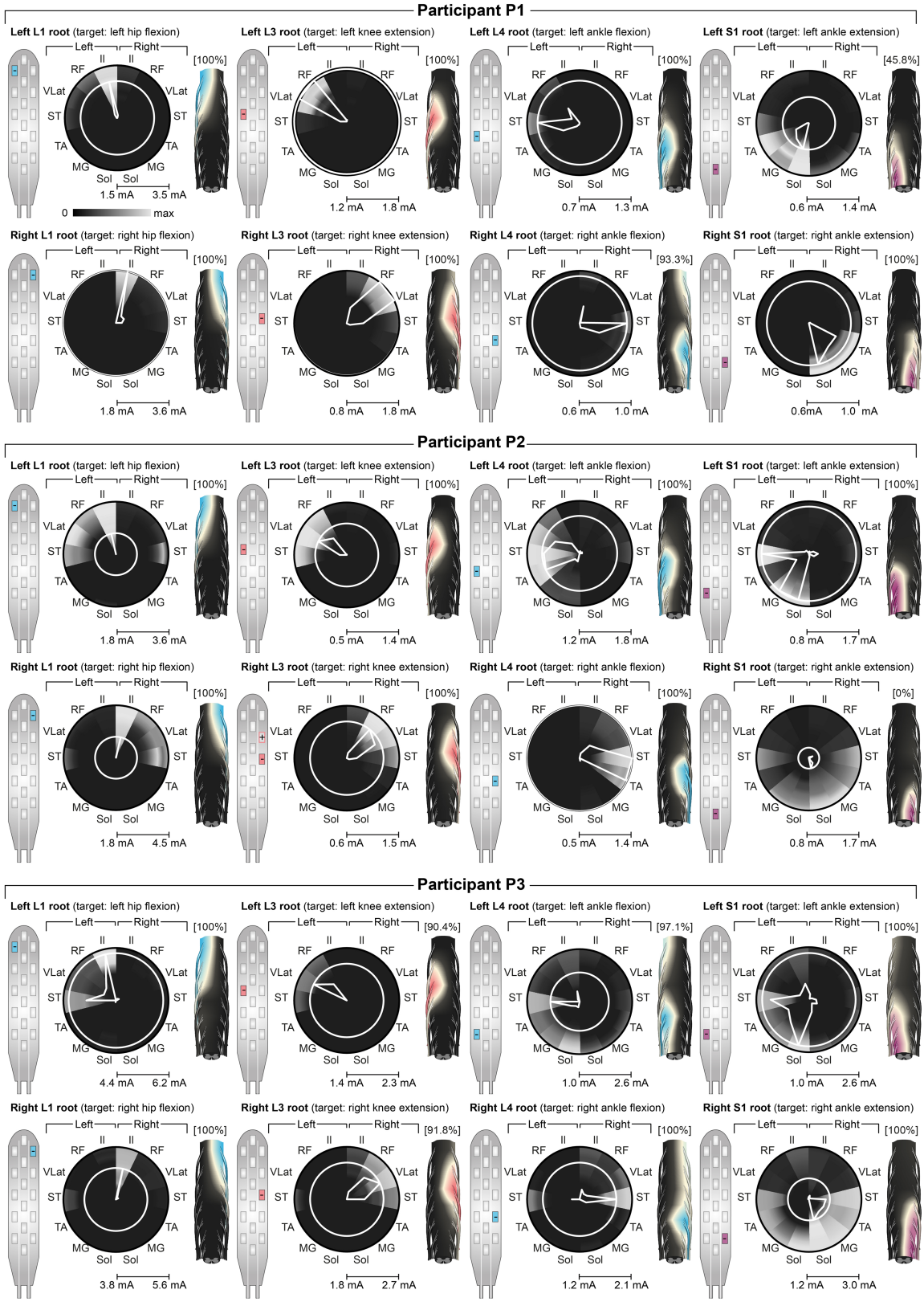

Extended Data Fig. 3 | Spatial selectivity of targeted electrode configurations. Monopolar configurations (shown on paddle array schematics) experimentally selected to target the left and right posterior roots associated with hip flexion (L1), knee extension (L3), ankle flexion (L4) and ankle extension (S1) for the three participants. The circular plots and motor neuron activation maps use the same conventions as in Fig. 2 and Extended Data Fig. 2 (median of $n = 4$ pulses). The normalized selectivity index is reported above each motor neuron activation map. This index represents the percentage of posterior root selectivity for the electrode configuration selected experimentally, with respect to the maximum posterior root selectivity that can be achieved among all monopolar configurations (all selectivity indices obtained from computational simulations). Note that in P2, the electrode selected experimentally to target the right S1 root was located on the midline and resulted in bilateral activation within computational simulations, which resulted in a normalized selectivity index of zero.

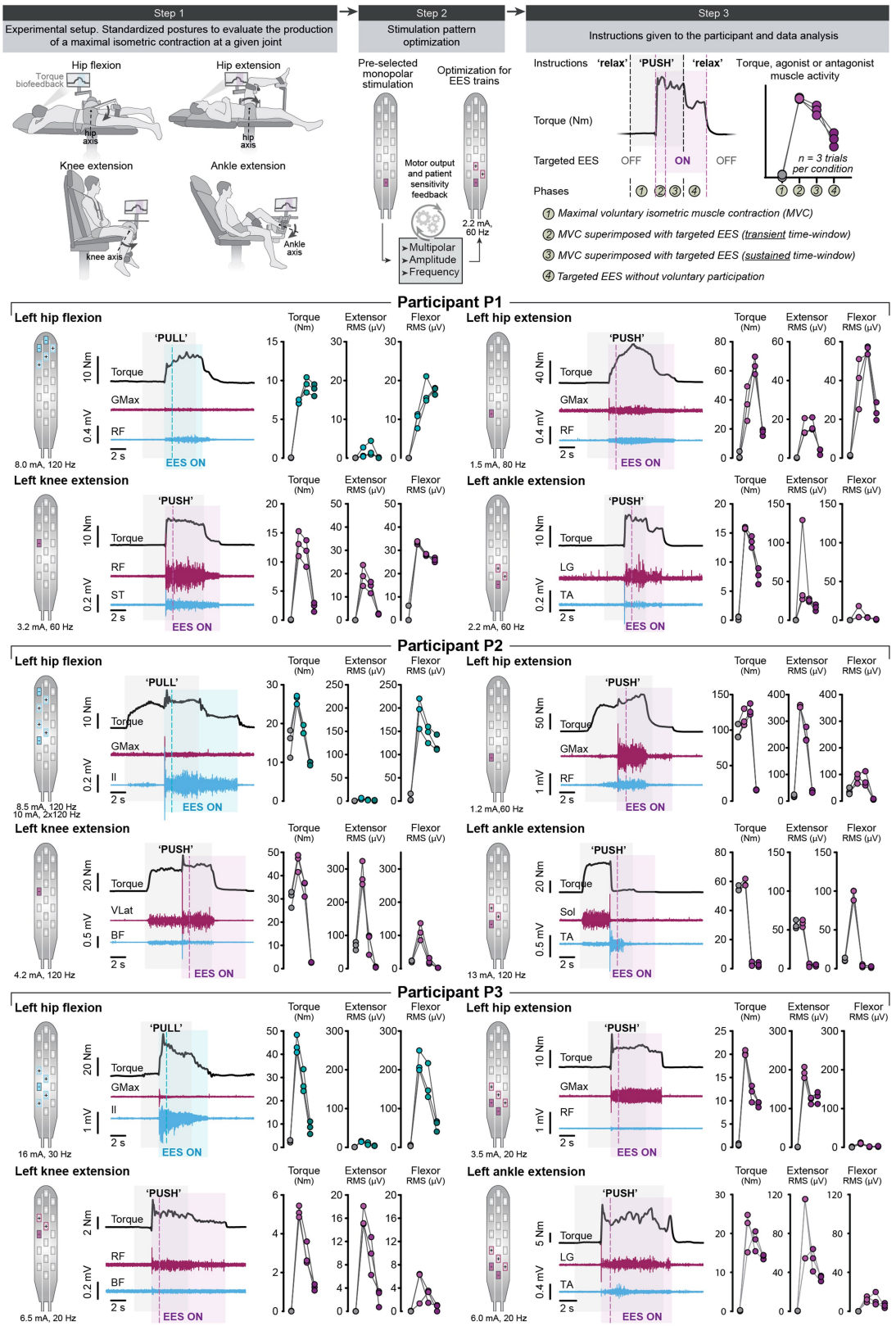

Extended Data Fig. 4 | See next page for caption.

Extended Data Fig. 4 | Single-joint movements enabled by targeted EES. Step 1: participants are placed in standardized positions to allow assessment of voluntary torque production at a single joint (isometric contractions) without and with targeted EES. Step 2: EES protocols elaborated from single-pulse experiments (Extended Data Figs. 2, 3) are optimized for each task using multipolar configurations and adjustments of EES amplitude and frequency. Step 3: sequence of each trial. Participants were asked to produce a maximal voluntary contribution, but failed in most cases, as evidenced by the absence of EMG activity during this period. While they continued trying to activate the targeted muscle, EES was switched on. After a few seconds, participants were instructed to stop their voluntary contribution. After a short delay, EES was switched off. For each sequence, the produced torque and EMG activity of the key agonist and antagonist muscles acting at the targeted joint were calculated over the four indicated phases of the trial. Plots report the measured torques and EMG activity during the various phase of the trial for the left legs of all participants for the four tested joints (cyan, flexor; magenta, extensor), together with EES parameters and electrode configurations. All measurements were performed before rehabilitation, except for hip extension in P1 and P2 (not tested before), and ankle extension in P3 (no capacity before rehabilitation), which were carried out after rehabilitation. Targeted EES enabled or augmented the specific recruitment of the targeted muscle, which resulted in the production of the desired torque at the targeted joint, except for ankle extension of P2. Plots show quantification of the EMG activity and torque for $n = 3$ trials per condition. Note that hip flexion can be enabled or augmented with EES targeting L1 and/or L4 posterior roots (heteronymous facilitation of flexor motor neuron pools).

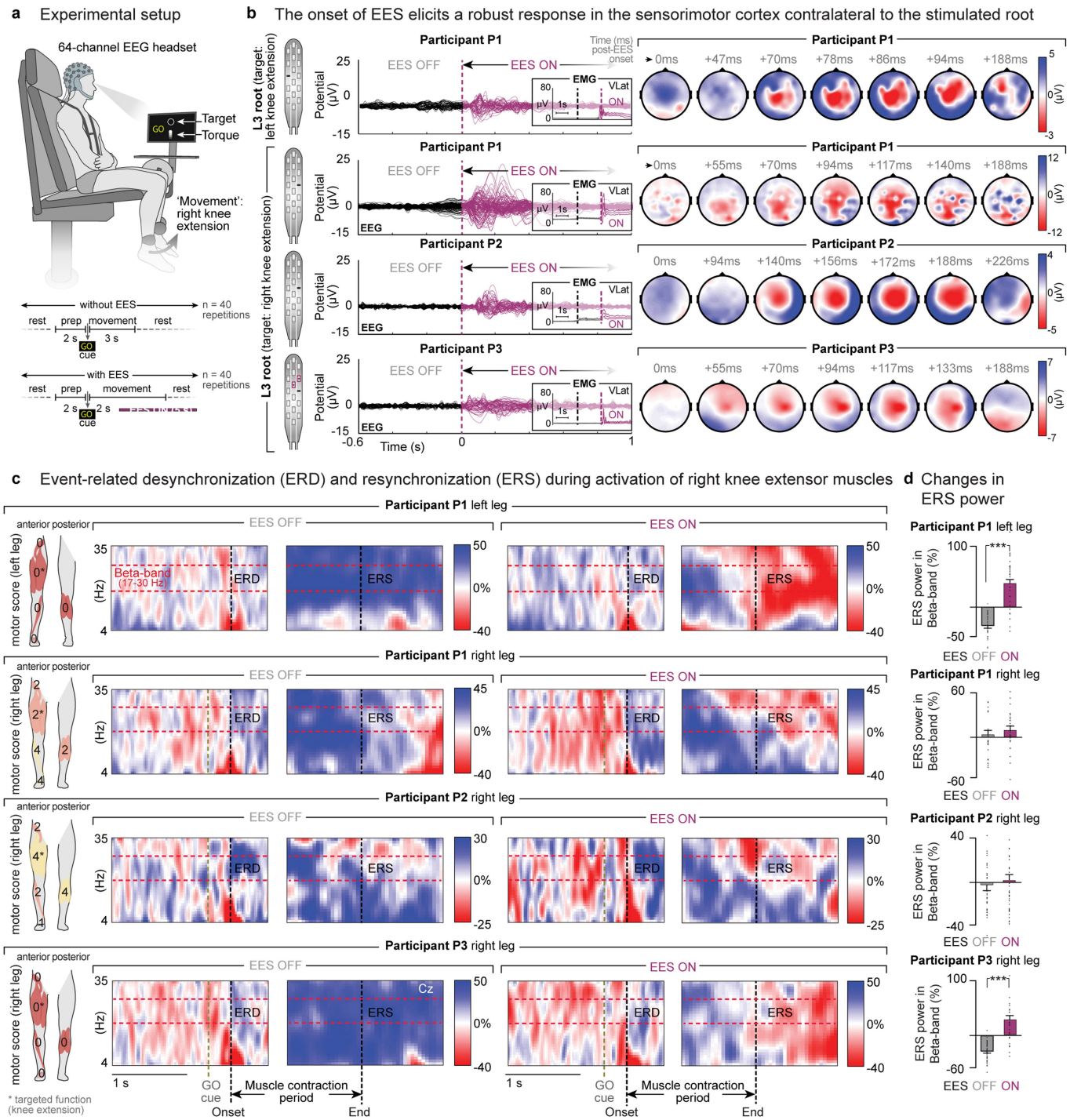

Extended Data Fig. 5 | Modulation of EEG activity during volitional contraction of leg muscles without and with EES. a, Recordings of EEG activity while participants were asked to produce an isometric torque at the knee joint without and with continuous EES targeting motor neuron pools innervating knee extensors, as shown in **b**. **b**, Superimposed EEG responses ($n = 40$ repetitions) and temporal changes in the topography of average activity over the cortical surface after the onset of EES, as indicated above each map. The onset was calculated from the onset of EMG responses in the targeted vastus lateralis muscle (insets). The stimulation elicited a robust event-related response over the left sensorimotor cortex with a latency of 90 ± 40 ms for P1 and P3, and of 170 ± 40 ms for P2 (full range of the peaks and middle of this range indicated). **c**, Average normalized time–frequency plots ($n = 40$ trials) showing ERD and ERS over the Cz electrode (central top electrode) for each individual during the voluntary activation of knee extensor muscles without and with EES. Schematic drawings (left) indicate the motor scores of the tested legs, including the targeted muscles (*), at the time of enrolment in the study. Both legs were tested in P1 owing to his asymmetric deficits. **d**, Normalized average power (mean ± s.e.m.) of the β-band over the Cz electrode during ERS from 0 to 500 ms after termination of contraction without and with continuous EES ($n = 40$ repetitions for each condition, individual data points shown except for outliers more than 3 median absolute deviations away from the median). $^{***}P < 0.001$ (permutation tests, see Methods).

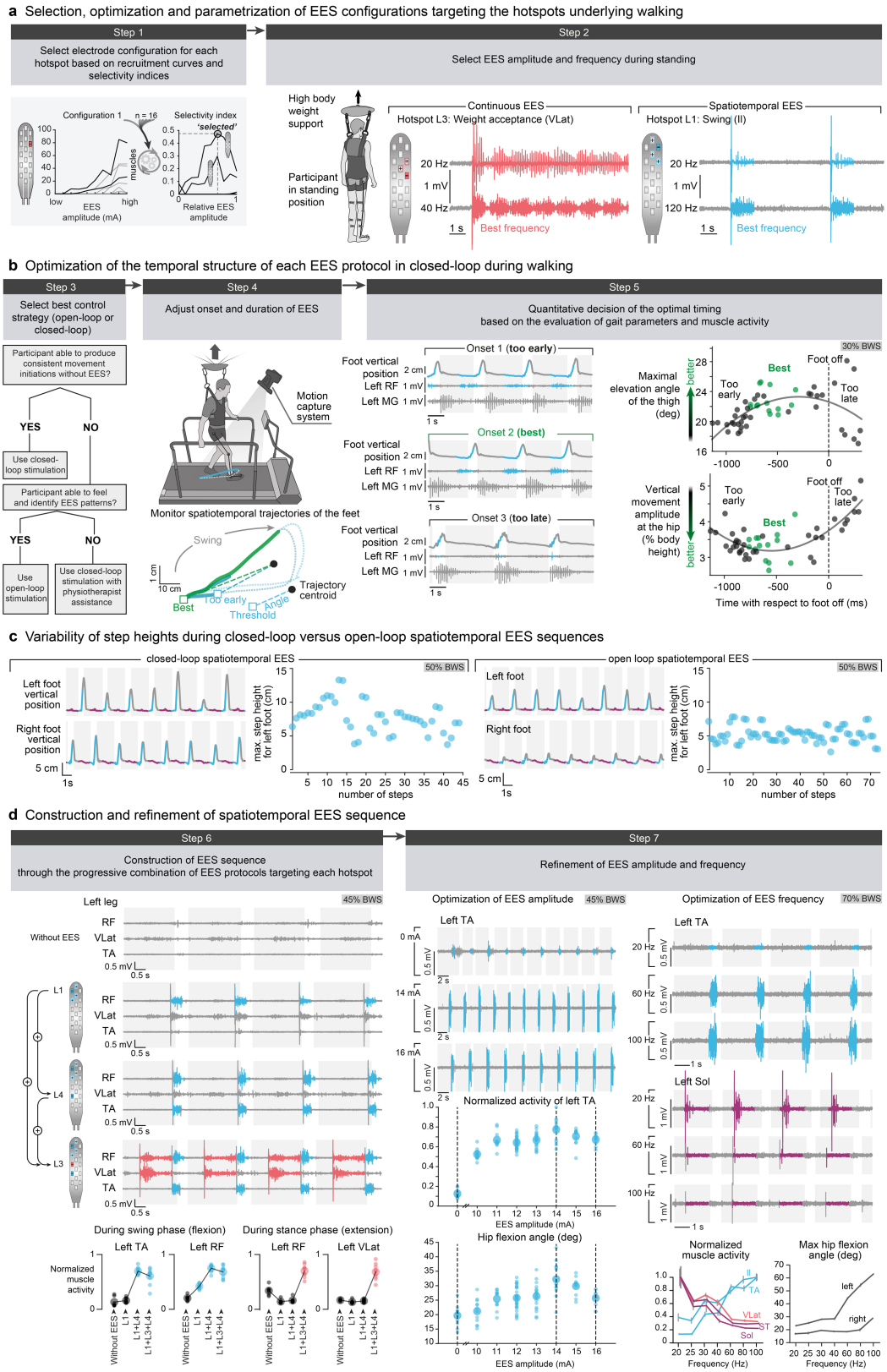

Extended Data Fig. 6 | See next page for caption.

Extended Data Fig. 6 | Configuration of spatiotemporal EES to enable walking. a, Spatial configuration. Step 1: select electrode configurations from single-pulse experiments to target the three hotspots underlying the production of walking in healthy individuals (weight acceptance: L3; propulsion: S1; swing: L1/L4). Step 2: optimize EES amplitude and frequency while delivering EES during standing. Multipolar configurations can be used to refine selectivity of EES protocols. Example shows continuous EES targeting the right L3 posterior root to facilitate right knee extension during standing, and trains (500 ms) of EES targeting the right L1 posterior root stimulation to facilitate hip flexion. Two EES frequencies are shown (P3). **b**, Temporal configuration. Step 3: decision tree to select the best strategy to configure the temporal structure of EES protocols. If the participant is able to initiate leg movements consistently, use closed-loop EES based on real-time processing of foot trajectory. If the participant is not able to initiate consistent leg movements but can feel when EES is applied, use open-loop EES. If the participant is not able to generate movement and cannot feel EES, use closed-loop EES combined with physiotherapist assistance to move the legs. Step 4: real-time monitoring of the spatiotemporal trajectory of the feet. The trajectory is modelled as a foot rotating in space around the centroid of the movement (updated every 3 s). Angular thresholds determine the onset and end of EES protocols. Step 5: example showing the effect of three different angular thresholds on the onset of EES and resulting kinematics and EMG activity, including the quantification of kinematics for each step and condition that enables selecting the optimal onset of EES trains (P1). The same approach is used to optimize the duration of each train. **c**, Comparisons between closed-loop and open-loop EES. Plots show the vertical displacements of the left and right feet and successive step heights during walking with spatiotemporal EES delivered in closed loop versus open loop, showing the reduced variability of step height during pre-programmed EES sequences (P1). **d**, Resulting EMG patterns. Step 6: example of the progressive addition of EES protocols targeting specific hotspots. Plots show the quantification of EMG activity for the displayed muscles ($n = 7$ gait cycles for no EES and $n = 9$ gait cycles for each stimulation condition, P2). Step 7: EES amplitudes and frequencies are adjusted to avoid detrimental interactions between the different EES protocols and thus obtain the desired kinematic and EMG activity. Plots report the modulation of EMG activity and kinematics with increases in EES amplitude and frequency (mean ± s.e.m.; amplitude data: $n = 10, 12, 12, 30, 19, 12, 11, 10$ gait cycles for amplitudes in increasing order, P2; frequency data: $n = 20, 15, 16, 17, 15, 16, 15$ gait cycles for frequencies in increasing order, P3).

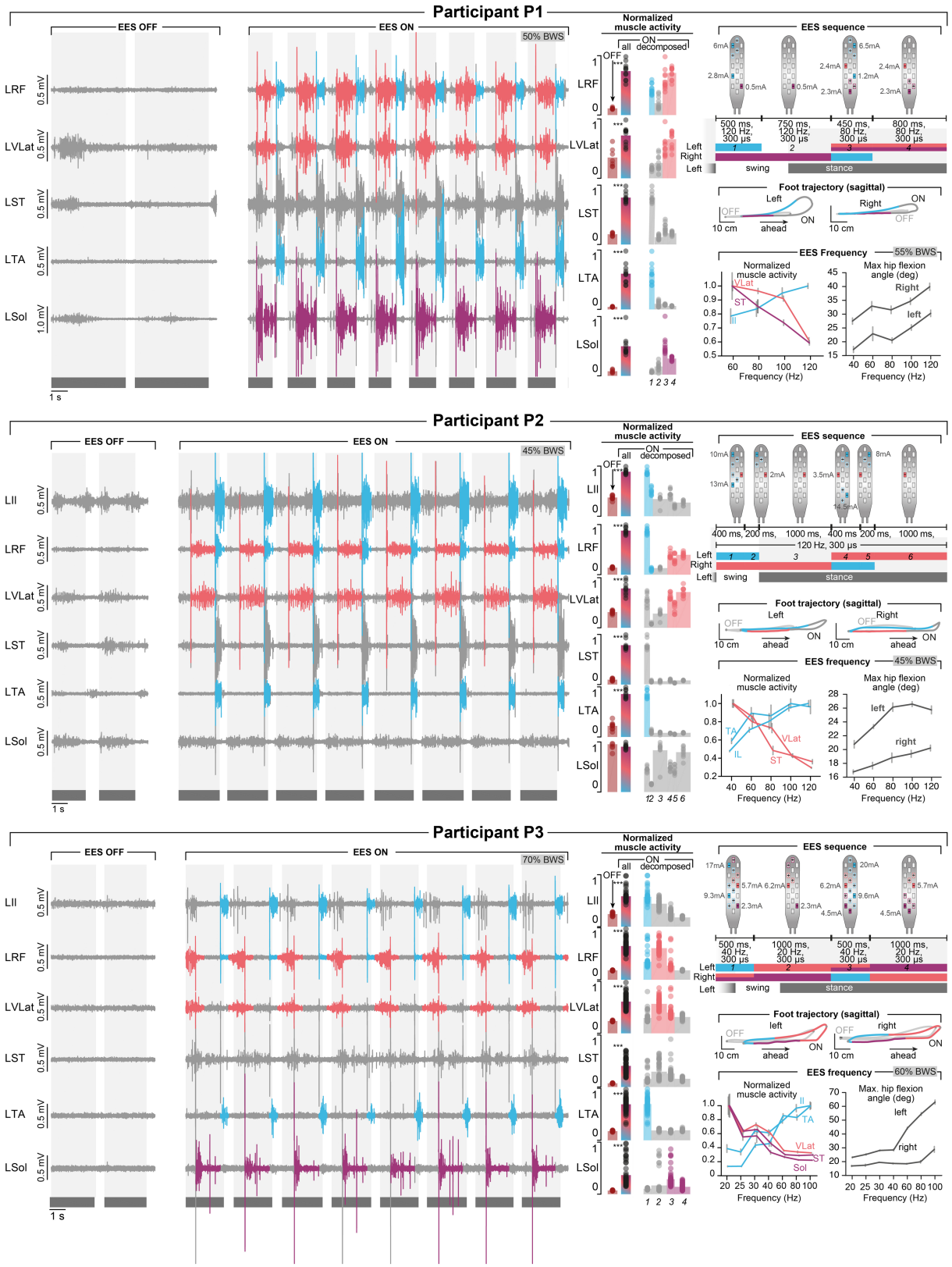

Extended Data Fig. 7 | See next page for caption.

Extended Data Fig. 7 | Targeted modulation of muscle activity during walking. Each panel reports the same representative data and quantification for one participant. Left, EMG activity of leg muscles during walking on a treadmill without EES (EES OFF) and with spatiotemporal EES (EES ON) while applying 50%, 45% and 70% body weight support for participants P1, P2 and P3, respectively. Stance and swing phases are indicated by grey and white backgrounds, respectively. The personalized spatiotemporal EES sequence (open loop) is schematized at the top right. The colours of each EES protocol refer to the targeted hotspots: weight acceptance (salmon), propulsion (magenta) and swing (cyan). These colours are used in the EMG traces to indicate the temporal window over which each targeted EES protocol is active. The bar plots report the amplitude of muscle activity without EES and with spatiotemporal EES, for which the quantification was performed over the entire burst of EMG activity and during each temporal window with targeted EES. The temporal windows are labelled with a number that refers to the spatiotemporal EES sequence. These results show the pronounced increase in the EMG activity of the targeted muscles (P1, no EES: $n = 7$ gait cycles, EES: $n = 11$ gait cycles; P2, no EES: $n = 9$ gait cycles, EES: $n = 9$ gait cycles; P3, no EES: $n = 10$ gait cycles, EES: $n = 57$ gait cycles). The average spatiotemporal trajectories of both feet with respect to the hip in the sagittal plane are shown for walking without EES and with spatiotemporal EES. The presence of targeted EES is indicated with the same colour code. Plots at bottom right show the relationships between EES frequency and the modulation of the EMG activity of flexor (blue) and extensor (magenta or salmon) muscles and maximum amplitude of hip movements during walking (mean ± s.e.m.; P1: $n = 14, 17, 15, 19$ gait cycles for increasing frequencies; P2: $n = 13, 16, 10, 17, 12$ gait cycles for increasing frequencies; P3: $n = 20, 15, 16, 17, 15, 16, 15$ gait cycles for increasing frequencies). $^{***}P < 0.001$. Student's t-test.

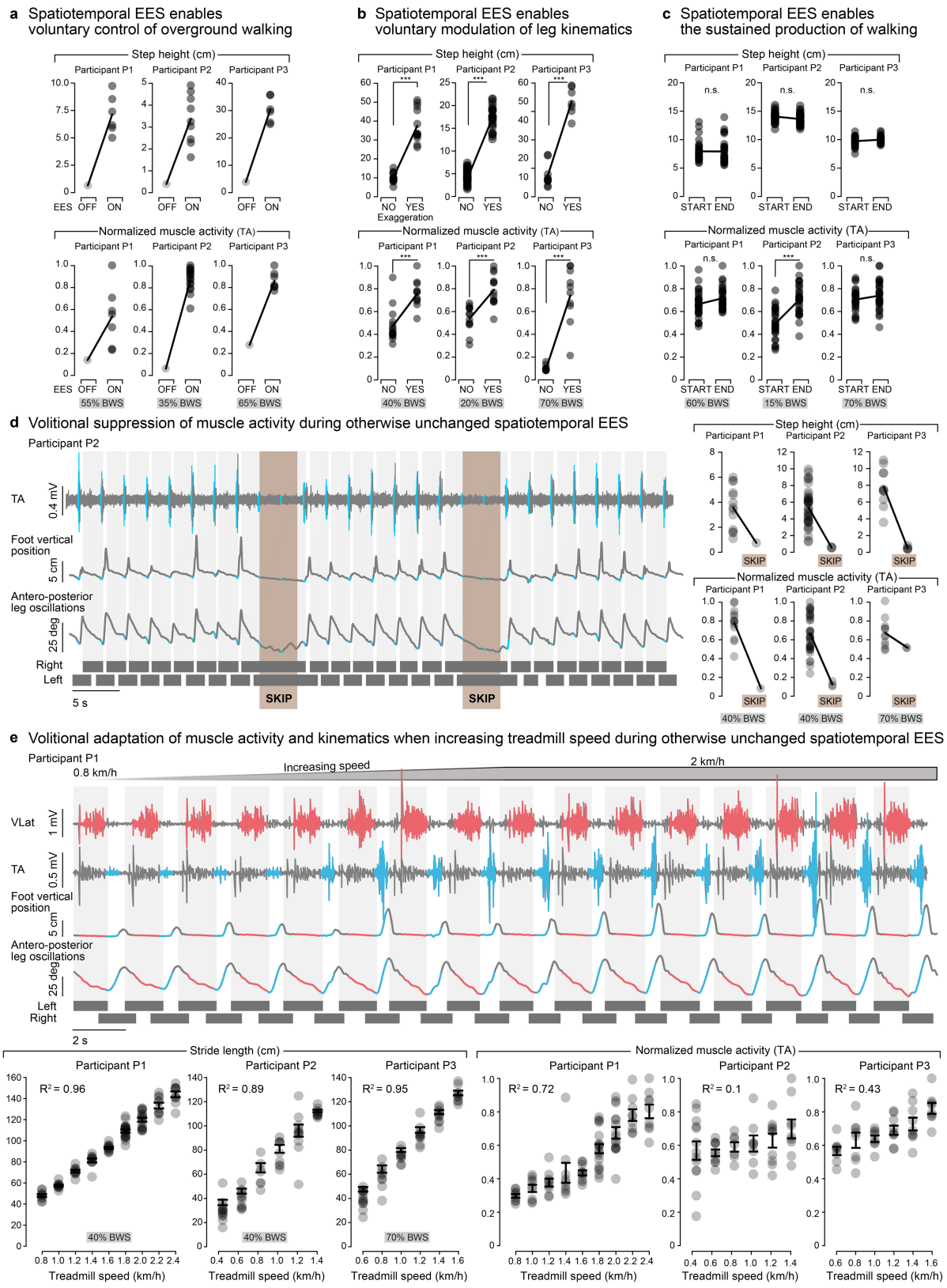

Extended Data Fig. 8 | See next page for caption.

Extended Data Fig. 8 | Volitional adaptations of walking during otherwise unchanged spatiotemporal EES. a–**c**, Quantifications of experiments shown in Fig. 4a–c for each participant. **a**, Step height and TA EMG activity with and without EES during overground walking (P1, EES ON: $n = 7$ gait cycles; P2, EES ON: $n = 16$ gait cycles; P3, EES ON, $n = 7$ gait cycles). **b**, Step height and TA EMG activity during normal steps and when participants were requested to perform exaggerated step elevations during overground walking (P1, $n = 15$ normal gait cycles, $n = 11$ exaggerated gait cycles; P2, $n = 31$ normal gait cycles, $n = 23$ exaggerated gait cycles; P3, $n = 14$ normal gait cycles, $n = 10$ exaggerated gait cycles). **c**, Step height and TA EMG activity during the first and last 30 steps extracted from a sequence of 1 h of locomotion on a treadmill ($n = 30$ gait cycles for all conditions). ***$P < 0.001$; n.s., non-significant; Student's *t*-test. **d**, EMG activity of representative leg muscles, vertical displacements of the foot and anteroposterior oscillations of the leg (virtual limb joining the hip to the foot) while P2 was walking continuously on the treadmill with spatiotemporal EES (open loop). The participant was asked to suppress the effects of EES and stand during one cycle of open-loop spatiotemporal EES sequence, highlighted in brown (SKIP), whereas he actively contributed to the production of movement the rest of the time. Plots report the quantification of step height and TA EMG activity during walking and when skipping steps for each participant (P1, $n = 13$ normal gait cycles, $n = 1$ skipped cycles; P2, $n = 36$ normal gait cycles, $n = 3$ skipped gait cycles; P3, $n = 11$ normal gait cycles, $n = 2$ skipped cycles). **e**, EMG activity of two representative muscles, vertical displacements of the foot and anteroposterior oscillations of the leg while P1 was walking on the treadmill and the speed of the belt increased progressively from 0.8 to 2 km h^{-1}. Plots show relationships between treadmill speed and mean stride length and TA EMG activity in all participants (P1: $n = 9, 9, 9, 9, 10, 18, 15, 9, 9$ gait cycles for increasing speeds; P2: $n = 13, 10, 7, 8, 10, 9$ gait cycles for increasing speeds; P3: $n = 8, 8, 10, 9, 9, 8$ gait cycles for increasing speeds; s.e.m. shown). The range of tested speeds was adapted to the walking ability of each participant.

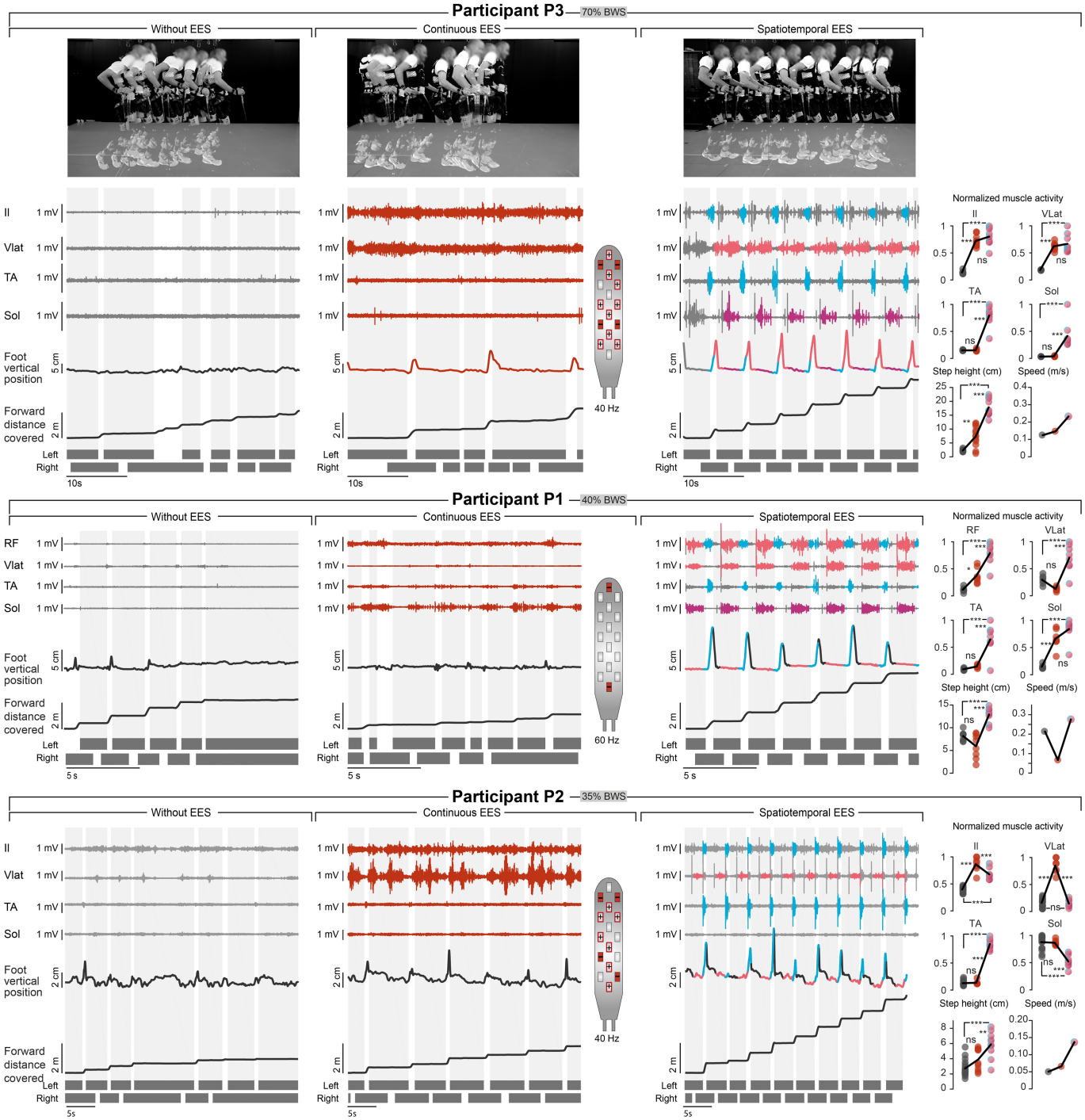

Extended Data Fig. 9 | Comparison between continuous and spatiotemporal EES during overground walking. Each panel represents one participant who is attempting to walk overground with gravity-assist without EES (left), with continuous EES (middle) and with spatiotemporal EES (right). EMG activity of representative leg muscles, vertical position of the foot and distance covered by the foot in the forward direction are displayed for each experimental condition. Continuous EES is applied throughout the trial (red). For P2 and P3, we optimized EES protocols that targeted the posterior roots on both sides, whereas EES was applied over the most rostral and most caudal midline electrodes for P1, as shown next to each plot. Spatiotemporal EES is represented using the same colour scheme as in Fig. 3 and Extended Data Fig. 7. The plots report quantification of EMG activity, step height and mean speed (based on distance covered) for the three experimental conditions (P1, $n = 6, 7, 8$ gait cycles for no EES, continuous EES and spatiotemporal EES; P2, $n = 17, 7, 9$ gait cycles for no EES, continuous EES and spatiotemporal EES; P3, $n = 6, 10, 9$ gait cycles for no EES, continuous EES and spatiotemporal EES). $^{***}P < 0.001$; $^{**}P < 0.01$; n.s., non-significant. One-way ANOVA, post hoc Tukey's HSD. These recordings were repeated on at least three different days for each participant.

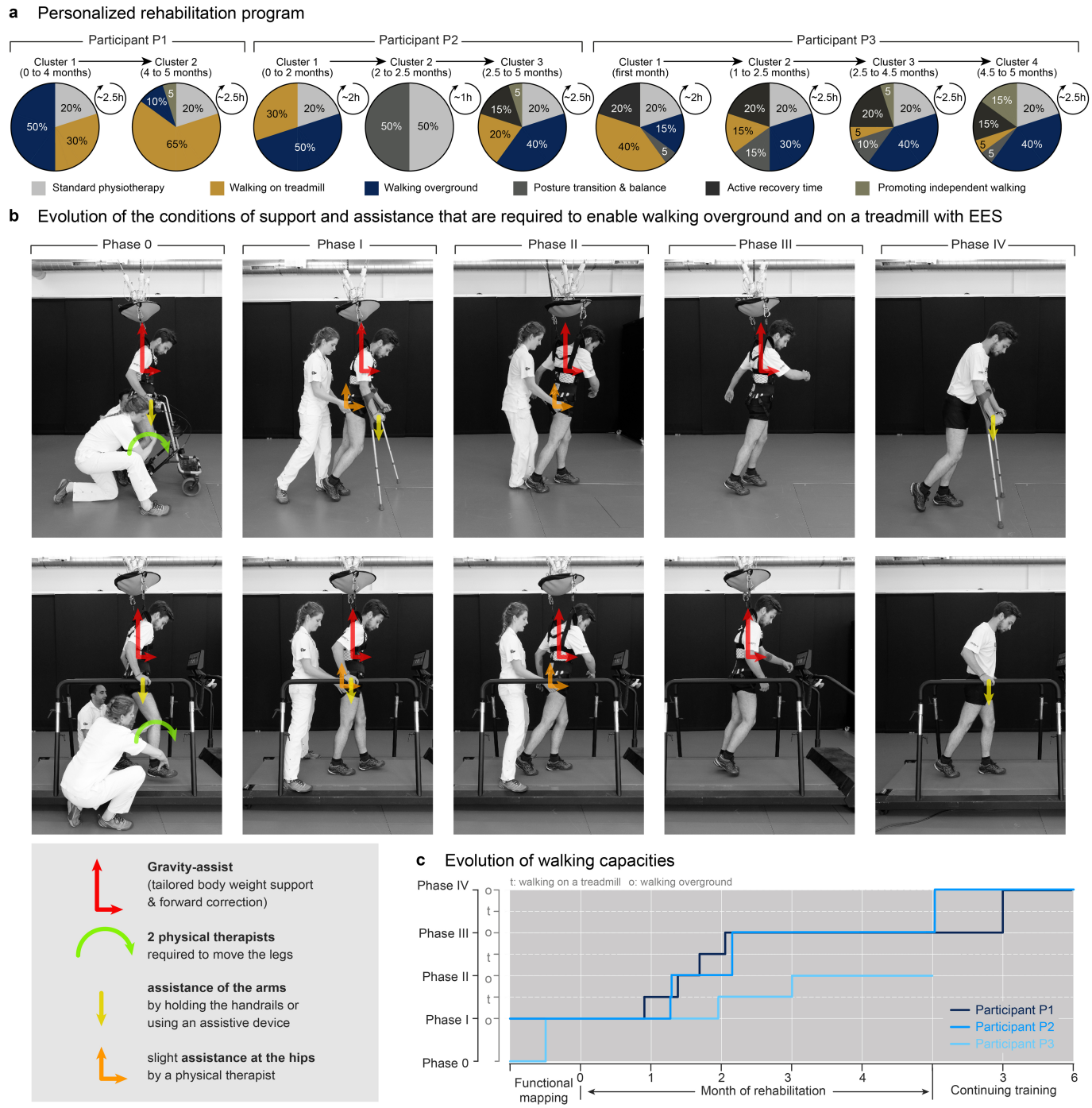

Extended Data Fig. 10 | Rehabilitation program and evolution of walking capacity. a, Rehabilitation programs were continuously personalized on the basis of the current motor performance of participants. Walking capacities evolved in phases (**b**). For this reason, the relative percentage of training in the various tasks has been divided into clusters, which correspond to the evolution of walking capacities. To facilitate the sustained production of reproducible locomotor movements (Extended Data Fig. 6c), EES was delivered in open-loop mode during gait rehabilitation. **b**, Walking capacities evolved through stereotypical phases that are illustrated in the snapshots. **c**, Plots showing the progression of the three participants along the phases of recovery during the rehabilitation program, and during the subsequent 6 months for P1 and P2. P3 had just completed the rehabilitation program at the time of submission of this study. See also Supplementary Video 4.

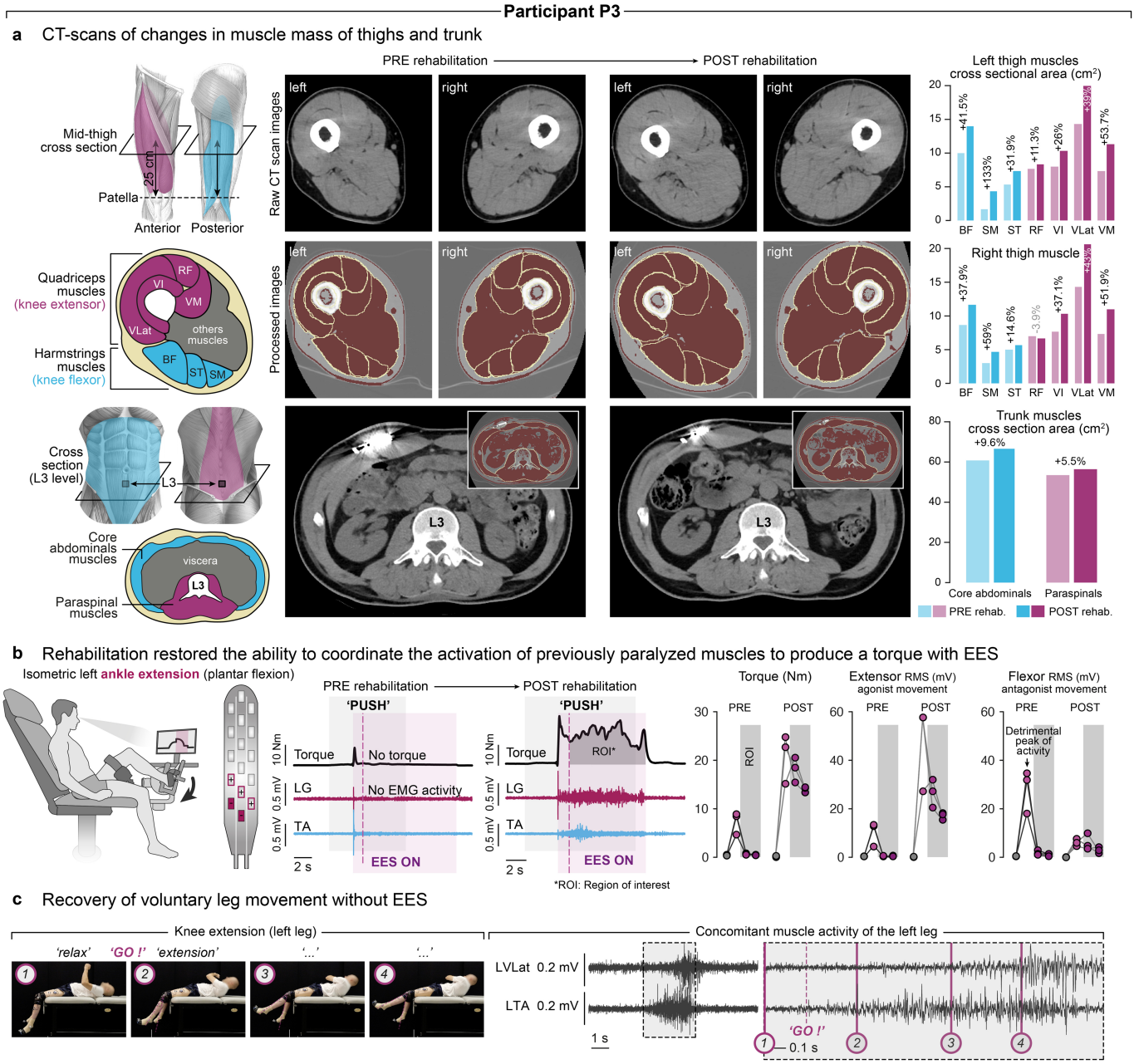

Extended Data Fig. 11 | Changes in muscle mass and quality and recovery of voluntary movements with and without EES in participant P3. a, Skeletal muscle mass and quality were assessed at the pre- and post-rehabilitation time points using X-ray attenuation from CT images obtained at the abdomen (L3 vertebra) and mid-thigh (25 cm above femorotibial joint space). Muscle mass was determined by measuring the cross-sectional areas (CSAs) of muscle tissues, while muscle quality was reflected by CT attenuation numbers (in Hounsfield units, HU) within the CSAs. Muscle segmentations were performed semi-automatically using ImageJ and muscle-specific HU thresholds (–29 to 150 HU). Plots report the substantial changes in muscle mass at mid-thigh, for both flexor and extensor muscles, and of trunk muscles. Muscle quality was also improved at both levels: total mid-thigh, left: 52.9 to 56.1 HU, right: 51.9 to 56.7 HU; total L3, 45.9 to 48.3 HU. This increase in CT attenuation numbers between the baseline CT scan and the follow-up imaging reflected the decrease in muscle fibre lipid content at the mid-thigh and abdomen. These evaluations were part of a protocol amendment obtained when enrolling P3. **b**, Assessment of voluntary torque production at the ankle (extension) with targeted EES before and after rehabilitation. Conventions are as in Extended Data Fig. 4. **c**, Snapshots showing voluntary extension of the left leg against the direction of gravity together with the concomitant sequence of EMG activity in the extensor and flexor muscles of this leg. The zoomed window shows the relationship between the movement and the EMG activity, indicated with the numbers. This participant presented flaccid paralysis, and had thus no control over leg muscles before the surgery. This movement was observed repeatedly at the end of the rehabilitation period (at least two days per week for several weeks).

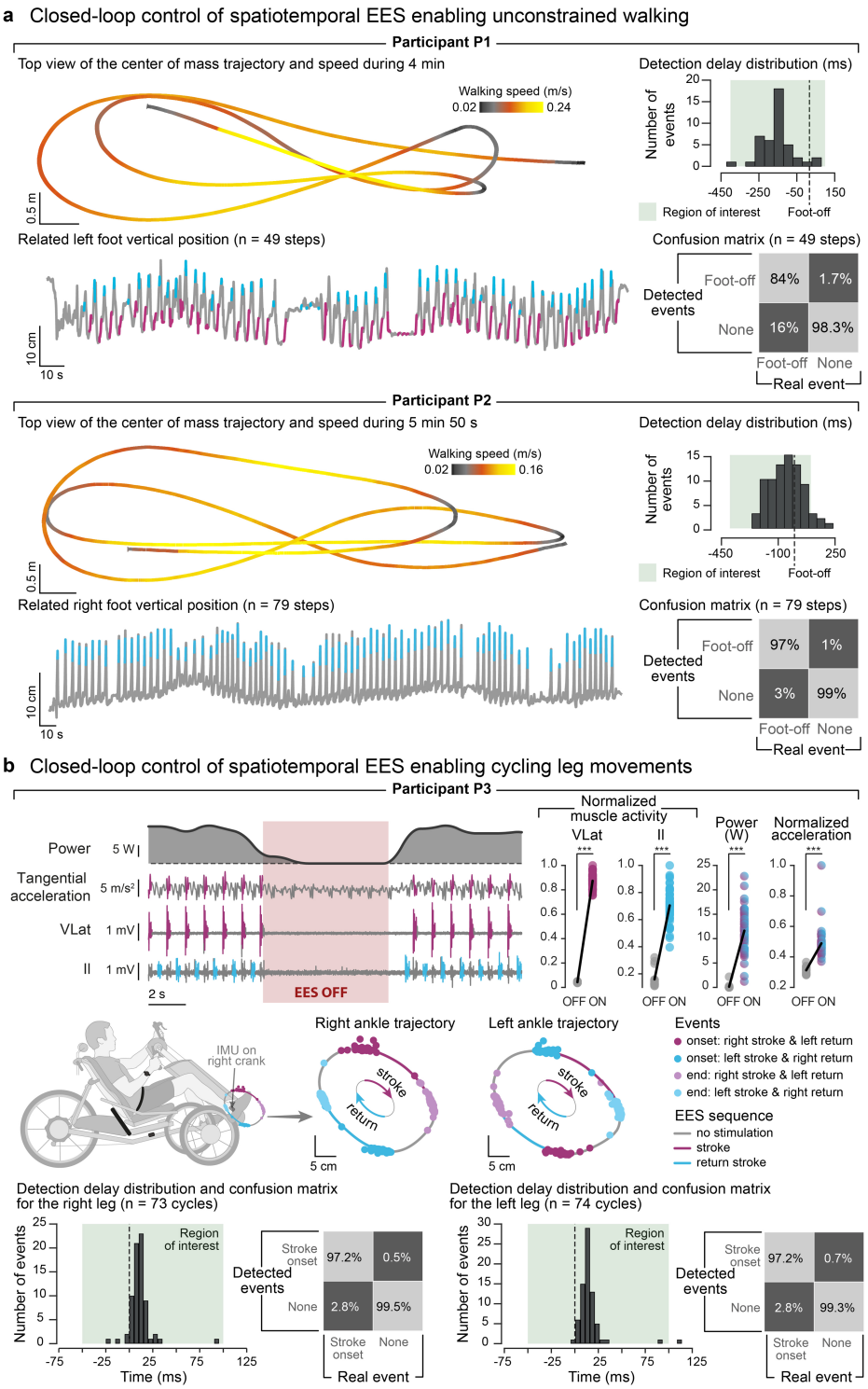

Extended Data Fig. 12 | Performance of closed-loop spatiotemporal EES to enable walking and cycling outside the laboratory. a, P1 and P2 were asked to walk freely overground with a walker (no body weight support) for 6 min. The concomitant vertical displacements of the foot show the consistency of EES triggering events despite variable foot kinematics and voluntary breaks. The trajectory of the centre of mass is shown from a top view to illustrate the ability to steer locomotion along any desired path. EES protocols took into account the deficits of each participant (cyan, EES targeting hip flexion; magenta, EES targeting knee and ankle extension). Histograms indicate the number of detected foot-off events for the represented leg as a function of the latency with respect to real foot-off events. The confusion matrix associated with these detections is represented below, as a percentage of the real events that were correctly or incorrectly classified. Detections were considered valid if they occurred between 400 ms before and 100 ms after real foot-off events, as highlighted in green on histograms (P1, $n = 49$ gait cycles; P2, $n = 79$ gait cycles). **b**, Closed-loop spatiotemporal EES was delivered in P3 using an electric trike powered by hand and foot pedals. Traces show EMG activities of the targeted hip flexor and knee extensor muscles on one leg together with the tangential acceleration of the pedal and power generated at the foot pedal. Plots report the quantification of flexor and extensor EMG activities, peak tangential accelerations and generated power without and with EES. Successive ankle trajectories during cycling are shown together with the timing of EES protocols targeting the hip flexor and knee extensor muscles. The histograms and confusion matrices report the performance of the controller following the same conventions as in **a**, except that the correct detection window was restricted to 50 ms before and 100 ms after the desired crank position (P3: $n = 73$ pedalling cycles). $^{***}P < 0.001$. Student's t-test.

Extended Data Table 1 | Neurological statuses of participants

Participant		P1		P2		P3	
Gender		m		m		m	
Age (y)		28		35		47	
Years after SCI		6		6		4	
Assessments at study enrollment (Pre) and after rehabilitation period (Post)		Pre	Post	Pre	Post	Pre	Post
Walking index for spinal cord injury (WISCI II score; max. 20)		13	16	6	13	0	0
American Spinal Injury Association Impairment Scale (AIS)		C	D	D	D	C*	C
Neurological level of injury		C7	C8	C4	C4	C7	C7
Upper Extremity Motor Scores:							
C5, elbow flexors	(right | left)	5 | 5	5 | 5	5 | 5	5 | 5	5 | 5	5 | 5
C6, wrist extensors	(right | left)	5 | 5	5 | 5	5 | 4	4 | 4	5 | 5	5 | 5
C7, elbow extensors	(right | left)	5 | 5	5 | 5	4 | 4	4 | 4	5 | 4	5 | 5
C8, finger flexors	(right | left)	4 | 4	5 | 4	1 | 0	3 | 1	4 | 4	4 | 5
T1, finger abductors	(right | left)	4 | 4	4 | 4	3 | 0	3 | 0	4 | 4	4 | 4
(max. 5 per side)							
Total (max. 50)		46	47	31	33	45	47
Lower Extremity Motor Scores:							
L2, hip flexors	(right | left)	2 | 0	4 | 2	2 | 2	3 | 2	0 | 0	0 | 1
L3, knee extensors	(right | left)	2 | 0	4 | 3	4 | 4	4 | 4	0 | 0	1 | 0
L4, ankle dorsiflexors	(right | left)	4 | 0	4 | 1	2 | 1	4 | 4	0 | 0	0 | 1
L5, long toe extensors	(right | left)	4 | 0	4 | 2	1 | 1	2 | 4	0 | 0	0 | 1
S1, ankle plantar flexors	(right | left)	2 | 0	4 | 2	4 | 4	5 | 4	0 | 0	0 | 0
(max. 5 per side)							
Total (max. 50)		14	30	25	36	0	4
Light Touch Sensory Scores:							
L1-S2 dermatomes subscore	(right | left)	7 | 7	7 | 7	5 | 8	2 | 10	1 | 4	2 | 5
(max. 14 per side)							
Total (max. 112)		75	76	65	71	55	57
Pin Prick Sensory Scores:							
L1-S2 dermatomes subscore	(right | left)	0 | 0	0 | 0	4 | 8	1 | 13	0 | 0	0 | 0
(max. 14 per side)							
Total (max. 112)		33	30	65	86	28	28

Subjects' neurological status according to the International Standards for Neurological Classification of Spinal Cord Injury at study entry and after completion of the five-month training program.
*Reason for AIS C classification in spite of motor scores of 0 throughout all lower extremity key muscles is the presence of voluntary anal contraction.

nature research

Corresponding author(s): Grégoire Courtine
gregoire.courtine@epfl.ch
Nature 2018-06-08551A

Reporting Summary

Nature Research wishes to improve the reproducibility of the work that we publish. This form provides structure for consistency and transparency in reporting. For further information on Nature Research policies, see Authors & Referees and the Editorial Policy Checklist.

Statistical parameters

When statistical analyses are reported, confirm that the following items are present in the relevant location (e.g. figure legend, table legend, main text, or Methods section).

n/a	Confirmed
☐	☒ The exact sample size (*n*) for each experimental group/condition, given as a discrete number and unit of measurement
☐	☒ An indication of whether measurements were taken from distinct samples or whether the same sample was measured repeatedly
☐	☒ The statistical test(s) used AND whether they are one- or two-sided *Only common tests should be described solely by name; describe more complex techniques in the Methods section.*
☐	☒ A description of all covariates tested
☒	☐ A description of any assumptions or corrections, such as tests of normality and adjustment for multiple comparisons
☐	☒ A full description of the statistics including central tendency (e.g. means) or other basic estimates (e.g. regression coefficient) AND variation (e.g. standard deviation) or associated estimates of uncertainty (e.g. confidence intervals)
☐	☒ For null hypothesis testing, the test statistic (e.g. *F*, *t*, *r*) with confidence intervals, effect sizes, degrees of freedom and *P* value noted *Give P values as exact values whenever suitable.*
☒	☐ For Bayesian analysis, information on the choice of priors and Markov chain Monte Carlo settings
☒	☐ For hierarchical and complex designs, identification of the appropriate level for tests and full reporting of outcomes
☐	☒ Estimates of effect sizes (e.g. Cohen's *d*, Pearson's *r*), indicating how they were calculated
☐	☒ Clearly defined error bars *State explicitly what error bars represent (e.g. SD, SE, CI)*

Our web collection on statistics for biologists may be useful.

Software and code

Policy information about availability of computer code

Data collection	EMG system: Myon 320, Myon AG, Schwarzenberg, Switzerland Motion capture system: Vicon Nexus software v1.8.5, Vicon Motion Systems, Oxford, UK Data acquisition system: Twincat 3.1, Beckhoff Automation GmbH & Co. KG, Huelshorstweg 20 33415 Verl Germany Custom C++ code to control stimulation in real-time inside the laboratory environment Custom C# code to control stimulation in real-time outside the laboratory environment Microsoft Visual Studio Professional 2012 (for development in C++) Microsoft Visual Studio Community 2017 (for development in C#)
Data analysis	Custom code in MATLAB R2018a used for all data analysis Kinematic analysis performed using Vicon Nexus software v1.8.5, Vicon Motion Systems, Oxford, UK Sim4Life v3.4 ImageJ 1.52

For manuscripts utilizing custom algorithms or software that are central to the research but not yet described in published literature, software must be made available to editors/reviewers upon request. We strongly encourage code deposition in a community repository (e.g. GitHub). See the Nature Research guidelines for submitting code & software for further information.

Data

Policy information about availability of data

All manuscripts must include a data availability statement. This statement should provide the following information, where applicable:

- Accession codes, unique identifiers, or web links for publicly available datasets
- A list of figures that have associated raw data
- A description of any restrictions on data availability

Data that supports the findings and software routines developed for the data analysis will be made available upon reasonable request to the corresponding author at gregoire.courtine@epfl.ch.

Field-specific reporting

Please select the best fit for your research. If you are not sure, read the appropriate sections before making your selection.

☒ Life sciences ☐ Behavioural & social sciences ☐ Ecological, evolutionary & environmental sciences

For a reference copy of the document with all sections, see nature.com/authors/policies/ReportingSummary-flat.pdf

Life sciences study design

All studies must disclose on these points even when the disclosure is negative.

Sample size	We report proof-of-concept results in three patients who contributed to a First-in-Man study. No previous data existed to predetermine sample size. Previous studies employing spinal cord stimulation or novel implanted neurotechnologies (e.g. brain machine interface) in individuals with spinal cord injury reported their results in 1 to 4 participants.
Data exclusions	No data were excluded from the analyses.
Replication	Reproducibility of the experimental findings was verified across several steps, several recording sessions and between all 3 participants.
Randomization	Randomization was not sought in the present study. Each participant served as his own control (stimulation off vs. on conditions; evaluations at different points over time throughout the rehabilitation training period)
Blinding	Investigators were not blinded. Their expertize was required to optimize the intervention and to apply the intervention during evaluations. Furthermore, the effects of the intervention were obvious, acutely producing changes in the kinematics and muscle activities of the participants during walking.

Reporting for specific materials, systems and methods

Materials & experimental systems

n/a	Involved in the study
☒	☐ Unique biological materials
☒	☐ Antibodies
☒	☐ Eukaryotic cell lines
☒	☐ Palaeontology
☒	☐ Animals and other organisms
☐	☒ Human research participants

Methods

n/a	Involved in the study
☒	☐ ChIP-seq
☒	☐ Flow cytometry
☐	☒ MRI-based neuroimaging

Human research participants

Policy information about studies involving human research participants

Population characteristics	Three male individuals, aged 28-47 y, all with a traumatic cervical spinal cord injury participated in the study. All participants had completed standard of care rehabilitation following their injury and were in a chronic state, 4-6 y post-injury. All displayed low motor scores in the lower limbs or complete motor paralysis, which bound them to a wheelchair.
Recruitment	Participant recruitment was done via the clinicaltrial.gov website where the principal investigators' contact details were disclosed (NCT02936453). Patients and physicians contacted them directly to communicate their interest to participate or to

refer a patient to the STIMO study. The clinical study nurse communicated with the patients or the referring physician and reviewed the clinical status of the patient for compliance with the inclusion and exclusion criteria listed below. Patients meeting the inclusion criteria were given the study's flyer and the informed consent form to understand further their implications and involvement within this clinical study. The participants' selection was also based on their ability to live independently and their autonomy in their daily living activities.

Inclusion Criteria:

- Age 18-65 (women or men)
- Incomplete SCI graded as AIS C & D
- Level of lesion: T10 and above, based on AIS level determination by the PI, with preservation of conus function
- The intact distance between the cone and the lesion must be at least 60mm
- Focal spinal cord disorder caused by either trauma or epidural, subdural or intramedullary bleeding
- Minimum 12 months post-injury
- Completed in-patient rehabilitation program
- Able to stand with walker or 2 crutches
- Stable medical and physical condition as considered by Investigators
- Adequate care-giver support and access to appropriate medical care in patient's home community
- Agree to comply in good faith with all conditions of the study and to attend all required study training and visits
- Must participate in two training sessions before enrolment
- Must provide and sign Informed Consent prior to any study related procedures

Exclusion Criteria:

- Limitation of walking function based on accompanying (CNS) disorders (systemic malignant disorders, cardiovascular disorders restricting physical training, peripheral nerve disorders)
- History of significant autonomic dysreflexia
- Cognitive/brain damage
- Epilepsy
- Patient who uses an intrathecal Baclofen pump.
- Patient who has any active implanted cardiac device such as pacemaker or defibrillator.
- Patient who has any indication that would require diathermy.
- Patient who has any indication that would require MRI.
- Patient that have an increased risk for defibrillation
- Severe joint contractures disabling or restricting lower limb movements.
- Haematological disorders with increased risk for surgical interventions (increased risk of haemorrhagic events).
- Participation in another locomotor training study.
- Congenital or acquired lower limb abnormalities (affection of joints and bone).
- Women who are pregnant (pregnancy test obligatory for woman of childbearing potential) or breast feeding or not willing to take contraception.
- Known or suspected non-compliance, drug or alcohol abuse.
- Spinal cord lesion due to either a neurodegenerative disease or a tumour.
- Patient has other anatomic or co-morbid conditions that, in the investigator's opinion, could limit the patient's ability to participate in the study or to comply with follow-up requirements, or impact the scientific soundness of the study results.
- Patient is unlikely to survive the protocol follow-up period of 12 months.

Magnetic resonance imaging

Experimental design

Design type	clinical structural MRI
Design specifications	N/A
Behavioral performance measures	N/A

Acquisition

Imaging type(s)	structural
Field strength	3 Tesla
Sequence & imaging parameters	Scanning sequence: TSE (Turbo Spin Echo) SPACE (Sampling Perfection with Application optimized Contrasts using different flip angle Evolution), imaging type: Cartesian, field of view: 200 mm x 200 mm, matrix size: 320 pixels x 320 pixels, slice thickness: 1 mm, orientation: axial, TE: 133 ms, TR: 1500 ms, flip angle: 125 degrees
Area of acquisition	spine

Diffusion MRI ☐ Used ☒ Not used

Preprocessing

Preprocessing software	N/A

Normalization: N/A

Normalization template: N/A

Noise and artifact removal: N/A

Volume censoring: N/A

Statistical modeling & inference

Model type and settings: N/A

Effect(s) tested: N/A

Specify type of analysis: ☐ Whole brain ☐ ROI-based ☐ Both

Statistic type for inference (See Eklund et al. 2016): N/A

Correction: N/A

Models & analysis

n/a	Involved in the study
☒	☐ Functional and/or effective connectivity
☒	☐ Graph analysis
☒	☐ Multivariate modeling or predictive analysis